Mg-Fe isotopes trace the mechanism of crustal recycling and arc magmatic processes in the Neo-Tethys subduction zone

Long Chen[1], Dongyong Li[1], Jianghong Deng[2], Sanzhong Li[1], Ian Somerville[3], Yi-Xiang Chen[4], Zi-Fu Zhao[4], Wei An[5], and Xiao-Hui Li[1]

[1]Ocean University of China
[2]Institute of Oceanology, Chinese Academy of Sciences
[3]University College Dublin
[4]University of Science and Technology of China
[5]Hefei University of Technology

March 26, 2023

Abstract

The mechanism of crustal recycling in subduction zones has been a heated debate, and Mg–Fe isotopes may provide new constraints for this debate. This study reported the Fe–Mg isotope data for mafic plutonic rocks from the eastern and central Gangdese arc and their associated trench sediments in southern Tibet. The δ26Mg (–0.32 to –0.20(0.04 to 0.12and positive correlations with (87Sr/86Sr)i and (206Pb/204Pb)i values, but positive and negative correlations with εNd(t) and εHf(t) values, respectively. The Mg and Fe isotopic compositions (δ26Mg = –0.28 to –0.15comparable with the eastern ones, but they are not covariant with Sr–Pb–Nd–Hf isotopes. More importantly, the Fe–Mg isotopes for most of the arc rocks fall in between local trench sediments (δ26Mg = –0.61 to –0.30qualitative analyses and quantitative simulations suggest that while the Mg–Fe isotope variations in the eastern Gangdese arc rocks revealed the important role of source mixing between sediment-derived melts and peridotite, their variations in the central Gangdese arc rocks reflected the controlling effects of source mixing between carbonated serpentinite-derived Mg-rich fluid and peridotite and source melting. The good covariant relationships between Mg–Fe isotope and traditional geochemical tracers provide further evidence for the recycling of crustal materials in subduction zones via various types of slab-derived fluids and melts.

Hosted file

959190_0_art_file_10822197_rrxbx0.docx available at https://authorea.com/users/598741/articles/631175-mg-fe-isotopes-trace-the-mechanism-of-crustal-recycling-and-arc-magmatic-processes-in-the-neo-tethys-subduction-zone

Hosted file

959190_0_supp_10821324_rrxwqc.docx available at https://authorea.com/users/598741/articles/631175-mg-fe-isotopes-trace-the-mechanism-of-crustal-recycling-and-arc-magmatic-processes-in-the-neo-tethys-subduction-zone

Mg–Fe isotopes trace the mechanism of crustal recycling and arc magmatic processes in the Neo-Tethys subduction zone

Long Chen[1, 2, 3*], Dong-Yong Li[1*], Jiang-Hong Deng[4*], San-Zhong Li[1, 3], Ian Somerville[5], Yi-Xiang Chen[2], Zi-Fu Zhao[2], Wei An[6], Xiao-Hui Li[1, 3]

[1]Frontiers Science Center for Deep Ocean Multispheres and Earth System, Key Lab of Submarine Geosciences and Prospecting Techniques, Ministry of Education (MOE) and College of Marine Geosciences, Ocean University of China, Qingdao 266100, China.

[2]School of Earth and Space Sciences, University of Science and Technology of China, Hefei 230026, China.

[3]Laboratory for Marine Mineral Resources, Qingdao National Laboratory for Marine Science and Technology, Qingdao 266100, China.

[4]Center of Deep Sea Research, Institute of Oceanology, Center for Ocean Mega–Science, Chinese Academy of Sciences, Qingdao 266071, China.

[5]UCD School of Earth Sciences, University College Dublin, Belfield, Dublin 4, Ireland.

[6]School of Resources and Environmental Engineering, Hefei University of Technology, Hefei 230009, China.

Corresponding author: Long Chen (chenlong@ouc.edu.cn) ; Dong-Yong Li (lidongyong@ouc.edu.cn); Jiang-Hong Deng (jhdeng0507@163.com)

Key Points:

- The Mg–Fe isotope compositions of the Gangdese arc mafic plutonic rocks are closely connected to their associated trench sediments
- Good covariant relationships between Mg–Fe isotope and traditional geochemical tracers are found for mafic arc rocks for the first time
- Mg–Fe isotope provide further evidence for crustal recycling in subduction zones via various types of slab-derived fluids and melts

Abstract

The mechanism of crustal recycling in subduction zones has been a heated debate, and Mg–Fe isotopes may provide new constraints for this debate. This study reported the Fe–Mg isotope data for mafic plutonic rocks from the eastern and central Gangdese arc and their associated trench sediments in southern Tibet. The $\delta^{26}Mg$ (–0.32 to –0.20‰) and $\delta^{56}Fe$ (0.04 to 0.12‰) values of the eastern Gangdese arc rocks show negative and positive correlations with $(^{87}Sr/^{86}Sr)_i$ and $(^{206}Pb/^{204}Pb)_i$ values, but positive and negative correlations with $\varepsilon_{Nd}(t)$ and $\varepsilon_{Hf}(t)$ values, respectively. The Mg and Fe isotopic compositions ($\delta^{26}Mg$ = –0.28 to –0.15‰; $\delta^{56}Fe$ = 0.02 to 0.12‰) of the central Gangdese arc rocks are comparable with the eastern ones, but they are not covariant with Sr–Pb–Nd–Hf isotopes. More importantly, the Fe–Mg isotopes for most of the arc rocks fall in between local trench sediments ($\delta^{26}Mg$ = –0.61 to –0.30‰; $\delta^{56}Fe$ = 0.00 to 0.17‰) and the normal mantle. Integrated qualitative analyses and quantitative simulations suggest that while the Mg–Fe isotope variations in the eastern Gangdese arc rocks revealed the important role of source mixing between sediment-derived melts and peridotite, their variations in the central Gangdese arc rocks reflected the controlling effects of source mixing between carbonated serpentinite-derived Mg-rich fluid and peridotite and source melting. The good covariant relationships between Mg–Fe isotope and traditional geochemical tracers provide further evidence for the recycling of crustal materials in subduction zones via various types of slab-derived fluids and melts.

Plain Language Summary

At present, the mechanism of crustal recycling in the subduction zone has been controversial, and magnesium and iron isotopes are considered potential tools to resolve this dispute. However, it is not straightforward to relate the Fe–Mg isotopic compositions of mafic arc rocks to specific crustal recycling processes, due to the lack of either good covariations between Fe–Mg isotopes and the traditional tracers such as radiogenic Sr–Pb–Nd–Hf isotopes, or the Fe–Mg isotope data for the intrinsically highly heterogeneous subducting sediments. We report the Fe–Mg isotope data for mafic plutonic rocks from the eastern and central Gangdese arc and their associated trench sediments in southern Tibet, and for the first time find good covariant relationships between Fe–Mg isotope compositions and traditional geochemical tracers of subduction zone processes in arc rocks. This finding, from the viewpoint of major element isotopes, provides further evidence for the recycling of crustal materials via various types of slab-derived fluids and melts rather than diapiric mélange in subduction zones.

1 Introduction

A subduction zone is the most important region for the transport of crustal materials to the mantle, although some of the subducted materials can be recycled to the crust via arc magmatism (e.g., Stern, 2002). Traditionally, crustal recycling in the subduction zone is thought to be accomplished by extraction of aqueous fluids and felsic melts, with characteristic trace-element fractionations from metasediments, subducted altered basaltic oceanic crust (AOC), as well as serpentinized lithospheric mantle (e.g., Ellam and Hawkesworth, 1988; Elliot, 2003; Elliot et al., 1997; Gill, 1981; Rüpke et al., 2004; Tatsumi et al., 1986). This idea has been widely accepted because, in addition to their success in explaining the isotopic characteristics of arc rocks (e.g., Hawkesworth et al., 1997; Miller et al., 1994; Morris et al., 1990; Nebel et al., 2011), experimental work (e.g., Hermann and Rubatto, 2009; Kessel et al., 2005; Skora and Blundy, 2010) demonstrated that subducted sediments partial melting together with AOC

dehydration can release liquids with the required unique trace-element fractionations for arc rocks (i.e., depleted in HFSEs, but enriched in LILEs; Elliot et al., 1997; Pearce and Peate, 1995). Nevertheless, this traditional wisdom has recently been challenged by renewed interest in the idea that a mélange composed of physically mixed slab metasediments, AOC, as well as hydrated mantle wedge, can rise from the cold interface of the mantle and slab into the hot shallow mantle wedge due to density buoyance and subsequently melt for arc magmatism (e.g., Codillo et al., 2018; Cruz-Uribe et al., 2018; Nielsen and Marschall, 2017).

The current arguments in support of the mélange model are based mostly on trace elements and their pertinent radiogenic or stable isotopes, therefore, whether this idea can withstand the examination of stable isotopes of major elements would be the key to further establishing the theoretical framework of crustal material recycling in subduction zones. Oxygen isotopes have been documented to be useful in discriminating different slab lithologies, especially sediments with exclusively heavy oxygen isotope composition than the normal mantle. Nevertheless, it is challenging to use oxygen isotopes to distinguish solid protoliths from their derivate fluids/melts that are generated under subduction zone conditions, because both have similar oxygen contents and isotope compositions (e.g., Bindeman, 2008; Eiler et at., 2000).

Mg and Fe isotopes are likely to provide new constraints on this issue because (1) the Mg and Fe contents are quite different between subducted slab lithologies and their derivate fluids/melts (e.g., Herman and Rubatto, 2009; Kessel et al., 2005; Rapp et al., 1999; Scambelluri et al., 2015); and (2) it is generally believed that the isotopically heterogeneous AOC (e.g., Huang et al., 2018; Rouxel et al., 2003), subducting sediments (e.g., Hu et al., 2017; Nebel et al., 2015), and abyssal peridotites (e.g., Beinlich et al., 2014, 2018; Chen et al., 2016; Debret et al., 2016; Liu et al., 2017) can be delivered to the mantle by subduction, since limited isotope fractionation is observed during slab dehydration/melting (El Korh et al., 2017; Huang et al., 2020; Inglis et al., 2017; Li D. Y. et al., 2016; Li, W. Y. et al., 2011, 2014; Wang, S. J. et al., 2014). Previous studies have revealed a negative correlation between δ^{57}Fe values and the slab thermal parameter φ (Foden et al., 2018), and a positive correlation between average δ^{26}Mg values and slab surface temperatures or slab depths (Hu et al., 2020) in global arc rocks. These observations verified the capability of Mg and Fe isotopes as tracers of slab materials recycling, though the exact meanings of these correlations are currently not very well understood (Foden et al., 2018; Hu et al., 2020). Specifically, Magnesium isotope is preliminarily used to trace the mechanism of serpentinite Mg recycling in subduction zones, and both serpentinite-derived fluids (Hu et al., 2020; Teng et al., 2016) and serpentinite themselves as part of a diapiric mélange (Hao et al., 2022) were claimed as the source for heavy Mg isotope components in arc magma sources. Mafic arc rocks generally show lighter Fe isotope signatures, compared to MORB (e.g., Dauphas et al., 2009; Foden et al., 2018; Nebel et al., 2015). It is proposed that these light values must result from either, the extraction melts with heavy Fe isotope from the peridotite sources, or the incorporation of materials with light Fe isotope from the slab, or a combination of both (e.g., Dauphas et al., 2009, 2017; Deng et al., 2022; Foden et al., 2018; Nebel et al., 2015), but the relative contribution of the two factors is currently not very clear. The main reason for this situation is that, while melt extraction would lead to the depletion of the mantle residual in heavy Fe isotope (e.g., Weyer and Ionov, 2007), the slab contribution is hard to be evaluated, because the subducting lithology, especially sediments, is highly variable in Fe isotopes and so far, no clear covariation between robust geochemical tracers of slab components and Fe isotope has been found to undisputedly constraint the direction of Fe isotope shifting of the mantle wedge in response to adding of slab materials (e.g., Deng et al., 2022; Foden et al.,

2018; Nebel et al., 2015). Nevertheless, simultaneous analyses of the Fe and radiogenic isotopes of the arc rocks and corresponding trench sediments show the potential to solve the above dilemma (e.g., Nebel et al., 2015). In addition, Fe isotopes are sensitive to both partial melting and source mixing (Dauphas et al., 2017), whereas Mg isotopes do not significantly change during partial melting (Teng et al. 2017). Therefore, integrated Mg and Fe isotopes analyses would be useful in discriminating the relative role and sequence of source mixing and partial melting, and thus the relative role of fluids/melts metasomatism and mélange diapirs in crustal recycling and arc magmatism.

In this study, both mafic plutonic rocks and their associated trench sediments from the Gangdese arc were analyzed for their Fe–Mg isotope compositions. Our new Fe–Mg isotope data exhibit good covariations with Sr–Pb–Nd–Hf isotope data and incompatible element ratios, providing solid evidence for the contribution of various fluids and melts from the slab to the mantle sources of arc rocks and their significant role on Fe–Mg isotope variation of arc magmas.

2 Geological setting and sampling

From south to north, the Neo-Tethyan subduction zone consists of the Xiukang Complex, the Indus-Yarlung Zangbo ophiolitic mélange zone, the Xigaze forearc basin, and the Gangdese continental arc (e.g., Dai et al., 2021; Hu et al., 2016, 2020; Yin and Harrison, 2000; Fig. 1).

The Gangdese arc is located at the central part of the >8000-km-long Neo-Tethyan arc system from Kohistan to Sumatra (Searle et al., 1987; Zhang et al., 2019), a product of the northward subduction of the Neo-Tethyan oceanic slab under the Lhasa terrane in the southernmost part of the Asian continent, from at least the Middle Triassic to the end of the Mesozoic (Zhu et al., 2019; Fig. 1a). The Lhasa terrane is classified into the northern, central, and southern subterranes, which are separated by the Shiquan River-Nam Tso Mélange Zone and Luobadui Milashan Fault, respectively (e.g., Zhu et al., 2011; Fig. 1b). The Gangdese arc magmatism is mainly confined to the Southern Lhasa subterrane (Fig. 1b) (Hu et al., 2016; Yin and Harrison, 2000; Zhu et al., 2019).

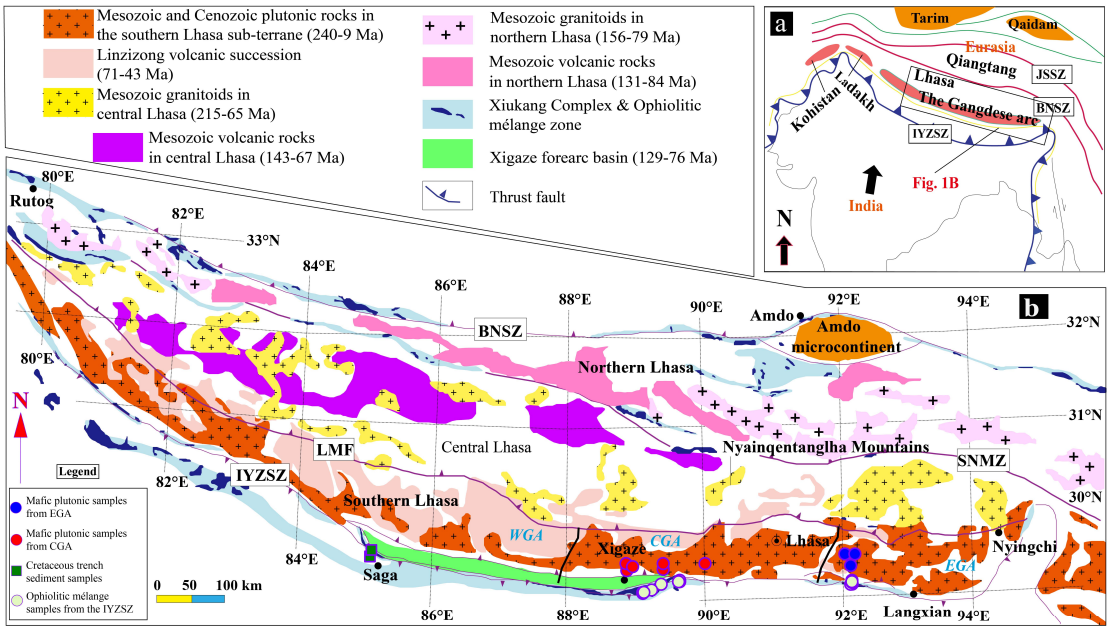

Figure 1. Tectonic framework and igneous rocks distribution in the Gangdese arc (modified from Zhu et al., 2019). (a) Location of the Gangdese arc in the Tibetan Plateau. (b) Distribution of the Mesozoic and Cenozoic plutonic and volcanic rocks in the Gangdese arc and the detailed sample locations for Late Cretaceous plutonic rocks and associated trench sediments that were investigated in the present study. Abbreviations: JSSZ = Jinsha Suture Zone; BNSZ = Bangong–Nujiang Suture Zone; SNMZ = Shiquan River–NamTso Mélange Zone; LMF = Luobadui–Milashan Fault; IYZSZ = Indus–Yarlung Zangpo Suture Zone; WGA = the Western Gangdese arc; CGA = the Central Gangdese arc; EGA = the Eastern Gangdese arc.

Arc magmatism has been dated to have started from the Middle Triassic and terminated around the Cretaceous-Tertiary boundary in the Gangdese arc with two tensive pulses at ca. 200–160 Ma and ca. 105–85 (Chen et al., 2022; Ji et al., 2009; Ma et al., 2013a, 2013b, 2013c; Wen et al., 2008; Zhang et al., 2010, 2014, 2020; Zhu et al., 2011, 2019). The existing arc rocks are composed of a large number of plutons with a small number of volcanic successions (Fig. 1b). The main products of the Cretaceous arc magmatism are gabbros/norites, diorites, granodiorites, with small amounts of ultramafic cumulates, including hornblendite, wehrlite, and dunite (Chen et al., 2022; Guo et al., 2020; Ma et al., 2013a, 2013b, 2013c; Zhang et al., 2020; Zhu et al., 2019). These plutons occur along a ~50-km-wide east-west striking narrow belt that is sub-parallel to the Indus Yarlung Zangbo Suture Zone (IYZSZ), from Xigaze in the central Gangdese arc (CGA; ~88–92° E) to Nyingchi in the eastern Gangdese arc (EGA; ~92–95° E) (Fig. 1b; Chen et al., 2022; Xu et al., 2015; Zhang et al., 2020).

Ophiolitic mélange zones in the IYZSZ are composed of both well-preserved and dismembered ophiolitic massifs, and were documented to have formed during the 130–120 Ma interval (e.g., Fig. 1b; Dai et al., 2021; Singh et al., 2022; Yin and Harrison, 2000). The prevailing view is that mafic rocks within these ophiolites formed in a forearc setting (Dai et al., 2021 and references therein), and therefore, their radiogenic isotope compositions can be treated as an analogy of the ambient subarc mantle (e.g., Chen et al., 2022; Ma et al., 2013a, 2013b, 2013c).

As summarized by Hu et al. (2020), the Xiukang Complex is traditionally considered to be a subduction complex that accreted on the Asian margin prior to the India-Asia collision. Nevertheless, recent field studies and provenance analyses have revealed that the Xiukang Complex formed during the Cretaceous to early Paleogene period, as a complex accretion product of the Neo-Tethyan subduction and the India-Asia collision. The recently established Cretaceous trench-fill deposits include the Luogangcuo, Rongmawa, and Jiachala formations. Since the depositional age of these trench sediments is contemporaneous with the Cretaceous intense pulse of magmatism in the Gangdese arc, these sediments can be used as recycled sediment end-members in the source region of these arc magmas (Chen et al., 2022).

In the present study, we have analyzed a series of mafic arc rocks, including diorites, gabbros, and norites from the Namling, Numa, and Nimu areas in CGA, as well as diorites and gabbros from the Zhengga area in the EGA (Fig. 1b). We also analyzed the Luogangcuo Formation paleo-trench sediments near Saga in the IYZSZ of southern Tibet, including conglomerate, coarse sandstone, and chert (Fig. 1b; An et al., 2018; Chen et al., 2022). The age, major-trace elements, and radiogenic Sr–Pb–Nd–Hf isotope compositions of the selected arc rocks and sediments have previously been analyzed by Chen et al. (2022). The results show that

trench sediment-derived melts were involved in the formation of most plutonic rocks, especially those of the EGA. Thus, we consider our sampled trench sediments representative of sediments that were incorporated in the mantle sources of the investigated Gangdese arc mafic rocks.

3 Analytical methods

Mg and Fe isotope analyses were performed at the Key Lab of Submarine Geosciences and Prospecting Techniques of the Ocean University of China, Qingdao. The procedures for sample dissolution, column chemistry, and instrumental analysis are described in detail by Dauphas et al. (2009) and Teng et al. (2010) and are summarized below. Approximately 50 to 70 mg of the same whole-rock powders as those used in Chen et al. (2022) were successively dissolved by concentrated (double-distilled) HF and HNO_3, HCl and HNO_3, as well as HCl in capped Savillex beakers (7 ml) using a hotplate. Once the dissolution was complete, the solution was evaporated to dryness before fluxing with 6N HCl for column chromatography.

3.1 Mg isotope analysis

Before chromatographic purification of Mg, about 0.2 to 0.6 ml of the stock solution was first dried, then evaporated with concentrated HNO_3, and finally digested with 1 ml 2 N HNO_3. Mg was then separated using 2 ml pre-cleaned AG50W-X8 (a Bio-Rad cation resin) that is conditioned with 1 N HNO_3. Matrix elements removal and Mg elution was done by 1 N HNO_3. About 20 mg Mg was loaded on the resin and the Mg was quantitatively extracted (>99% yields). Compared to the loaded Mg, the <10 ng blank of the whole procedure for Mg is negligible. The Mg contents in the elution collected before and after the Mg cuts were analyzed to assess the Mg yields. During column chemistry, basalt and andesite standards (JB-2 and JA-2) were processed along with our samples.

Mg isotope ratios were analyzed on a Neptune Plus Multi-Collector Inductively Coupled Plasma Mass Spectrometer (MC-ICPMS). The instrumental fractionation correction was done by sample-standard bracketing during measurement. Mg solutions were introduced with 2% HNO_3 under ‘‘wet” plasma conditions and analyzed in a low-resolution mode. Standard DSM3 was used to report Mg isotopic data: $\delta^{i}Mg = [(^{i}Mg/^{24}Mg)_{sample}/(^{i}Mg/^{24}Mg)_{DSM\text{-}3}–1] \times 1000‰$, i = 25 or 26. The associated error is 2SD for each datum, and the long-term external precision is ± 0.06‰ for $\delta^{26}Mg$. During our analyses, the basalt standard (JB-2) yield $\delta^{26}Mg$ of –0.23 ± 0.07‰, and the andesite standard (JA-2) yield $\delta^{26}Mg$ of –0.28 ± 0.03‰ (Table 1). These values agree well with the recommendations (Table 1).

3.2 Fe isotope analysis

Fe was purified using 1 ml pre-cleaned and 6 N HCl conditioned AG1-X8 (a Bio-Rad anion resin). The eluting of Fe was done by 0.4 N HCl after 10 ml 6 N HCl.

Fe isotope ratios were also analyzed on a Neptune Plus MC-ICPMS. The instrumental fractionation correction was done by sample-standard bracketing during measurement. Fe solutions were diluted by 2% HNO_3 to 2 ppm and bracketed with 2 ppm IRMM14. ^{57}Fe, ^{56}Fe, and ^{54}Fe were analyzed in static mode on H1, C, and L2 Faraday cups, respectively. Measurements were carried out in medium resolution (M/ΔM of 7000) using Sample + H cone with the ^{56}Fe sensitivity of ~7V/ppm. Fe standard IRMM14 was used to report Fe isotope: $\delta^{i}Fe = [(^{i}Fe/^{54}Fe)_{sample}/(^{i}Fe/^{54}Fe)_{IRMM14}–1] \times 1000‰$, i = 56 or 57. The associated error is 2SD for each datum, and the long-term external precision is ± 0.06‰ for $\delta^{56}Fe$. During our analyses, the basalt

standard (JB-2) yielded δ^{56}Fe of 0.05 ± 0.06‰, and the andesite standard (JA-2) yielded δ^{56}Fe of 0.13 ± 0.00‰ (Table 1). These values also agree well with recommendations (Table 1), verifying the accuracy of the methods.

Table 1

Fe-Mg isotope compositions of Gangdese arc rocks and trench sediments.

Categories	Sample ID	Lithology	SiO_2	MgO	CaO/Al_2O_3[c]	δ^{56}Fe	2σ	δ^{57}Fe	2σ	δ^{26}Mg	2σ	δ^{25}Mg	2σ
Standard reference material	JB-2	Basalt				0.05	0.05	0.06	0.08	-0.23	0.07	-0.13	0.02
	Recommended values[a]	Basalt				0.06	0.04	0.09	0.06	-0.21	0.02	-0.11	0.01
	JA-2	Andesite				0.13	0.00	0.14	0.02	-0.28	0.03	-0.14	0.05
	Recommended values[b]	Andesite				0.11	0.04	0.14	0.03	-0.29	0.00	-0.15	0.03
Gangdese arc trench sediments	12QD07	Sandstone	61.9	1.5	2.37	0.09	0.05	0.15	0.10	-0.61	0.00	-0.36	0.03
	12LGC19	Chert	89.7	0.3	2.04	0.17	0.04	0.31	0.08	-0.56	0.04	-0.27	0.00
	12LGC19 Re	Chert	89.7	0.3	2.04	0.15	0.01	0.23	0.03	-0.53	0.03	-0.31	0.05
	12QD18	Conglomerate	69.0	1.9	0.34	0.10	0.05	0.15	0.03	-0.37	0.01	-0.24	0.08
	12LGC02	Conglomerate	72.3	2.3	0.11	0.06	0.02	0.09	0.02	-0.42	0.03	-0.23	0.06
	12LGC13	Sandstone	60.6	2.2	0.59	0.02	0.05	0.03	0.10	-0.30	0.02	-0.17	0.01
	12LGC29	Pebbled coarse sandstone	72.2	1.5	0.09	0.00	0.05	0.03	0.07	-0.43	0.05	-0.24	0.02
Eastern Gangdese arc	15XZ254	Monzonite	57.6	3.5		0.07	0.05	0.17	0.11	-0.26	0.02	-0.16	0.04
	15XZ255	Monzonite	58.7	3.4		0.04	0.01	0.13	0.06	-0.23	0.01	-0.14	0.07
	15XZ259	Diorite	61.5	2.8		0.05	0.01	0.08	0.09	-0.24	0.01	-0.14	0.03
	15XZ263	Diorite	55.2	5.6		0.09	0.00	0.01	0.11	-0.22	0.06	-0.14	0.03
	15XZ286	Hornblende gabbro	46.0	5.7		0.12	0.03	0.24	0.13	-0.32	0.02	-0.20	0.02
	15XZ289	Gabbro	47.7	6.4		0.11	0.01	0.12	0.01	-0.28	0.03	-0.14	0.05
	15XZ291	Hornblende gabbro	41.2	13.7		0.09	0.01	0.17	0.06	-0.25	0.02	-0.22	0.03
	15XZ300	Gabbro	49.0	7.7		0.09	0.02	0.16	0.10	-0.20	0.01	-0.14	0.01
	15XZ301	Gabbro	49.8	12.0		0.07	0.00	0.13	0.05	-0.30	0.06	-0.19	0.00
Central Gangdese arc	15XZ482	Diorite	57.9	4.2		0.08	0.04	0.07	0.07	-0.28	0.02	-0.21	0.04
	15XZ483	Monzonite	57.3	4.5		0.05	0.05	0.06	0.06	-0.27	0.03	-0.14	0.00
	15XZ488	Monzonite	57.6	4.1		0.06	0.06	0.09	0.10	-0.23	0.02	-0.15	0.02
	15XZ492	Diorite	55.2	6.7		0.04	0.03	0.11	0.12	-0.24	0.04	-0.15	0.03
	15XZ494	Monzonite	59.0	3.8		0.08	0.02	0.10	0.09	-0.20	0.03	-0.12	0.02
	15XZ497	Monzonite	58.1	3.4		0.05	0.04	0.09	0.04	-0.25	0.06	-0.14	0.01
	15XZ503	Monzodiorite	55.8	3.9		0.06	0.05	0.12	0.10	-0.21	0.01	-0.14	0.00
	15XZ504	Monzodiorite	56.0	3.7		0.05	0.03	0.04	0.09	-0.27	0.02	-0.14	0.02
	15XZ510	Monzodiorite	54.6	4.1		0.05	0.03	0.03	0.10	-0.22	0.03	-0.14	0.02
	15XZ511	Monzodiorite	54.1	5.4		0.07	0.04	0.14	0.00	-0.15	0.01	-0.13	0.03
	15XZ514	Monzodiorite	53.8	4.6		0.07	0.00	0.05	0.10	-0.25	0.06	-0.16	0.06
	15XZ515	Monzodiorite	53.3	4.8		0.05	0.02	0.07	0.09	-0.19	0.00	-0.15	0.09
	15XZ516	Monzodiorite	54.3	4.3		0.05	0.07	0.10	0.09	-0.24	0.04	-0.11	0.00
	15XZ634	Monzodiorite	54.4	3.4		0.02	0.03	0.06	0.04	-0.22	0.00	-0.14	0.06
	15XZ643	Gabbro	46.5	8.0		0.11	0.05	0.15	0.09	-0.22	0.02	-0.09	0.01
	15XZ644	Gabbro	50.2	4.7		0.04	0.04	0.08	0.10	-0.25	0.05	-0.18	0.02
	15XZ644 Re	Gabbro				0.06	0.03	0.08	0.01	-0.16	0.04	-0.11	0.00
	15XZ645	Gabbro	51.2	4.3		0.05	0.07	0.13	0.05	-0.22	0.01	-0.13	0.01
	15XZ727	Hypersthene-bearing Diorite	56.1	3.8		0.05	0.03	0.19	0.13	-0.24	0.05	-0.14	0.02

Note. [a]Recommended values for Mg and Fe isotopes are from Teng et al. (2017) and He et al. (2015), respectively.[b]Recommended values for Mg and Fe isotopes are from Gao et al. (2019) and He et al. (2015), respectively.[c]CaO/Al_2O_3 ratios from Chen et al. (2022). Re = repeat column chemistry from another aliquot of dissolved sample solution.

4 Results

The Mg and Fe isotope compositions of the Gangdese arc rocks and associated trench sediments (Table 1) are illustrated in Fig. 2. The δ^{26}Mg values of the Gangdese arc rocks range from –0.32 to –0.15‰ with a weighted mean of –0.24 ± 0.01‰, δ^{56}Fe values range from 0.02 to 0.12‰ with a weighted mean of 0.07 ± 0.01‰, overlapping with part of the global arc rocks that show the relatively low δ^{26}Mg and high δ^{56}Fe values, respectively. While most of the arc rocks show Mg isotope composition overlapping with MORB, the δ^{56}Fe values for most arc rocks are lower than MORB but higher than mantle peridotite (Fig. 2). In general, EGA samples have comparable Mg and Fe isotope compositional ranges to those of the CGA, though the two groups of samples have different MgO and SiO_2 compositional ranges (Table 1 and Fig. 2).

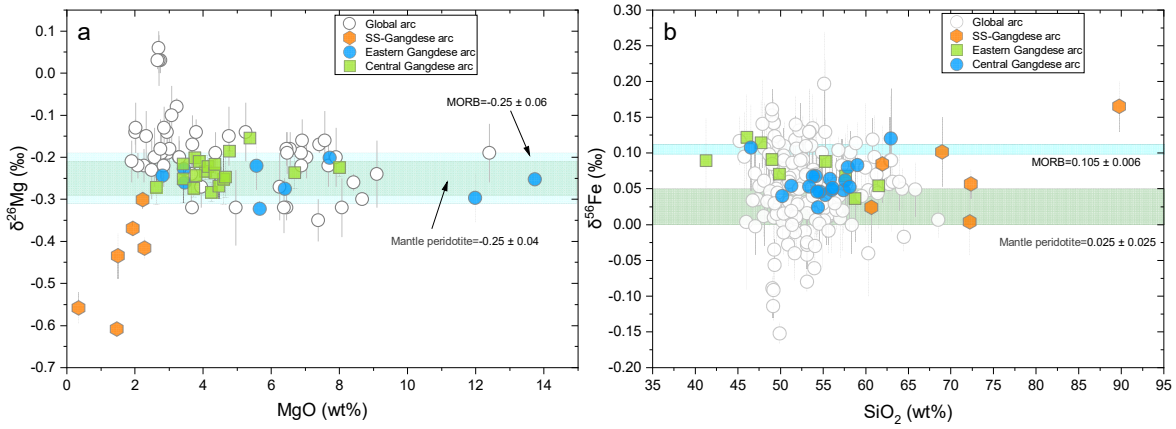

Figure 2. Fe–Mg isotope plots for the Gangdese arc rocks. (a) δ^{26}Mg vs. MgO; (b) δ^{56}Fe vs. SiO_2. The Mg isotope data for global arc rocks are from Teng et al. (2016) and Li, S. G. et al. (2017); The Fe isotope data for global arc rocks are from Dauphas et al. (2009), Nebel et al. (2015), Williams et al. (2018) and Foden et al. (2018); The Fe isotope data for Banda arc trench sediments, Indonesia (SS–Banda arc) are from Nebel et al. (2015). The Mg isotope values for mantle peridotite and MORB are adopted from Teng et al. (2010), and the Fe isotope values for mantle peridotite and MORB are adopted from Craddock et al. (2013) and Dauphas et al. (2017), respectively. Uncertainties are plotted at 2σ and are smaller than the symbols when not shown.

The Mg and Fe isotope composition of Gangdese arc sediments shows δ^{26}Mg and δ^{56}Fe ranges from –0.61 to –0.30‰, and 0.00 to 0.17‰, respectively (Fig. 2). In general, sediments with higher CaO/Al_2O_3 ratios tend to have lower δ^{26}Mg values (Table 1), suggesting the influence of the relative proportion of carbonate components on the Mg isotope compositions of the bulk rocks (Hu et al., 2017). The Mg isotope composition of Gangdese arc sediments overlaps the relatively light Mg isotope values observed for global subducting sediments (Hu et al., 2017; Teng et al., 2016), and five out of six of the sediments show δ^{26}Mg values lower than MORB, mantle peridotite as well as Gangdese arc rocks (Fig. 2a). On the other hand, the Fe isotope composition of Gangdese arc sediments overlap the Banda arc sediments (Nebel et al., 2015) with slightly larger compositional range extents to the lower δ^{56}Fe values (Fig. 2b), which also overlaps with Gangdese arc rocks, except for one sample that shows a higher δ^{56}Fe value

than all the arc rocks. Collectively, the sediments subducted along the Gangdese part of the Neo-Tethys subduction zone have light weighted mean Mg ($\delta^{26}Mg$ = –0.45 ± 0.10‰) and heavy weighted mean Fe ($\delta^{56}Fe$ = 0.07 ± 0.05‰) isotope compositions with restricted ranges.

5 Discussion

5.1 Covariations between Fe–Mg isotope and traditional tracers

When plotted against Sr–Pb–Nd–Hf isotope compositions in the isotope space (Figs. 3 and 4), the $\delta^{26}Mg$ values of EGA samples generally show a clear negative covariation with $(^{87}Sr/^{86}Sr)_i$ and $(^{206}Pb/^{204}Pb)_i$ ratios (Figs. 3a and 3c), but a positive covariation with $\varepsilon_{Nd}(t)$ and $\varepsilon_{Hf}(t)$ values (Figs. 3b and 3d); in contrast, the $\delta^{56}Fe$ values of these rocks show a positive covariation with $(^{87}Sr/^{86}Sr)_i$ and $(^{206}Pb/^{204}Pb)_i$ ratios (Figs. 4a and 4c), but a negative covariation with $\varepsilon_{Nd}(t)$ and $\varepsilon_{Hf}(t)$ values (Figs. 4b and 4d). These covariation patterns defined progressive variation trends from end-members with relatively heavy Mg isotope, light Fe isotope, and less enriched Sr–Pb–Nd–Hf isotopes to end-members with relatively light Mg isotope, heavy Fe isotope, and more enriched Sr–Pb–Nd–Hf isotopes (Figs. 3 and 4). On the other hand, the Mg and Fe isotopes of the CGA samples stretch out straight from the end-members with relatively heavy Mg isotope, light Fe isotope, and less enriched Sr–Pb–Nd–Hf isotope to lighter Mg and heavier Fe isotopes without changing of Sr–Pb–Nd–Hf isotope compositions (Figs. 3 and 4).

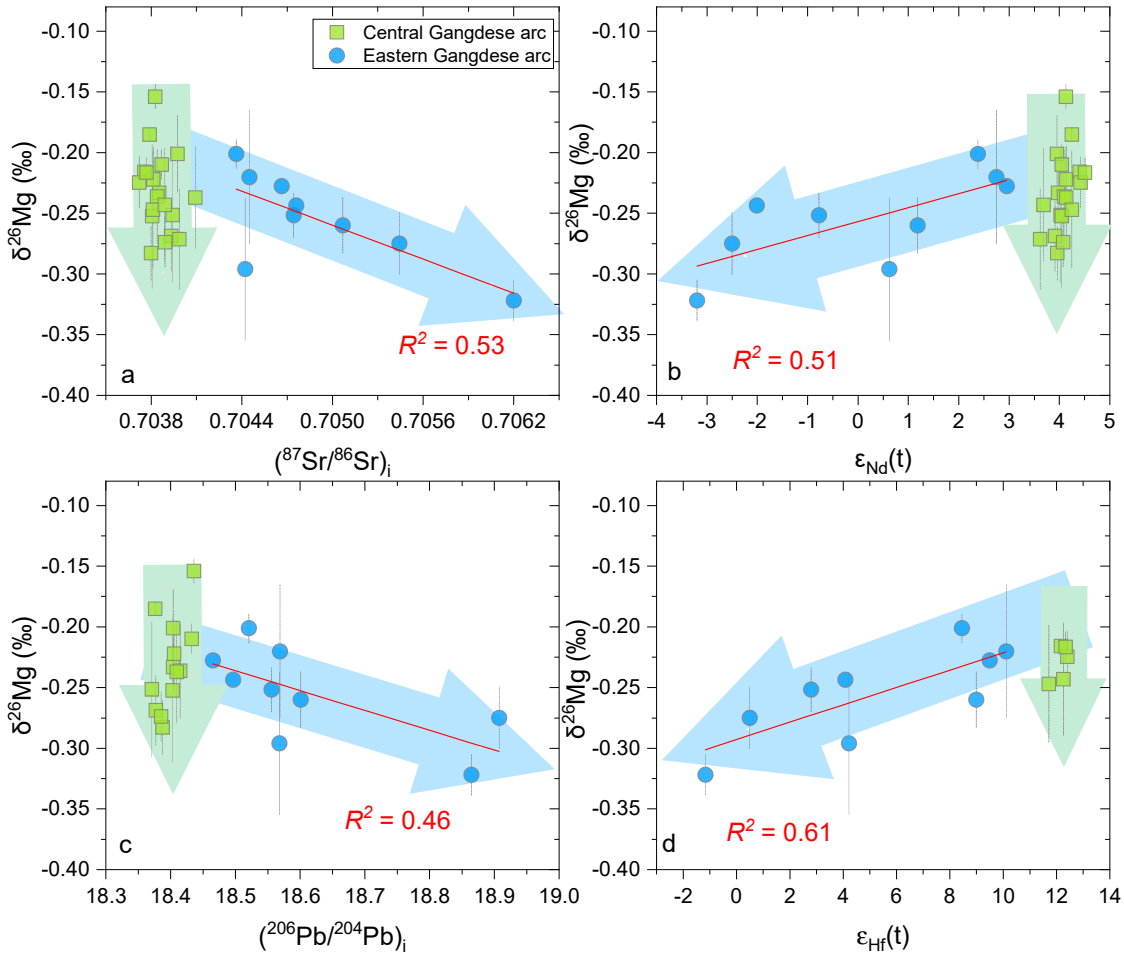

Figure 3. Mg isotope composition in comparison with Sr–Pb–Nd–Hf isotopes for the Gangdese arc rocks. (a) $\delta^{26}Mg$ vs. $(^{87}Sr/^{86}Sr)_i$; (b) $\delta^{26}Mg$ vs. $\varepsilon_{Nd}(t)$; (c) $\delta^{26}Mg$ vs. $(^{206}Pb/^{204}Pb)_i$; (d) $\delta^{26}Mg$ vs. $\varepsilon_{Hf}(t)$. The Sr–Pb–Nd–Hf isotope data are from Chen et al. (2022). R^2 denotes the values of R-Square that are reported by linear fit using Origin software.

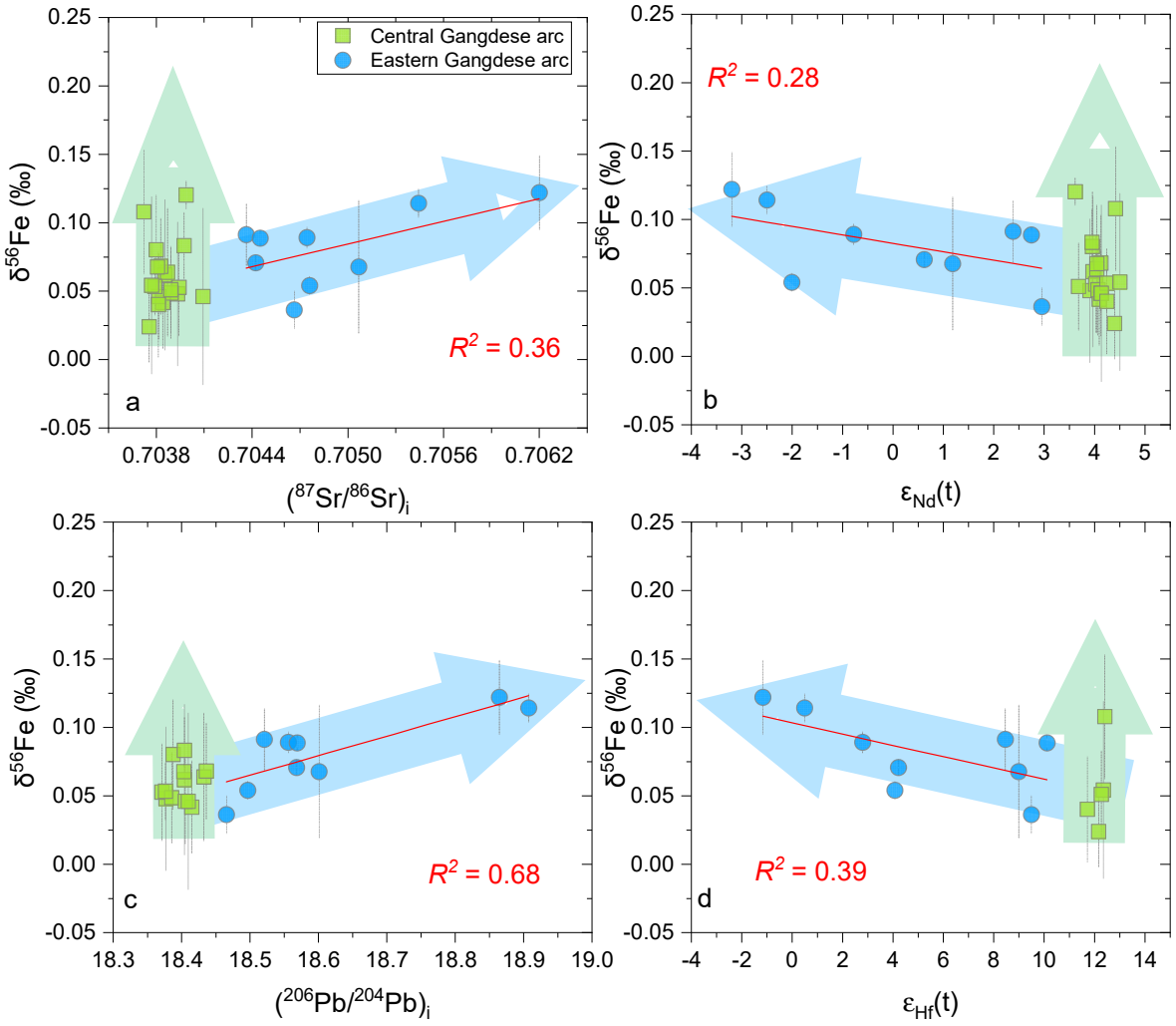

Figure 4. Fe isotope composition in comparison with Sr–Pb–Nd–Hf isotopes for the Gangdese arc rocks. (a) $\delta^{56}Fe$ vs. $(^{87}Sr/^{86}Sr)_i$; (b) $\delta^{56}Fe$ vs. $\varepsilon_{Nd}(t)$; (c) $\delta^{56}Fe$ vs. $(^{206}Pb/^{204}Pb)_i$; (d) $\delta^{56}Fe$ vs. $\varepsilon_{Hf}(t)$. The Sr–Pb–Nd–Hf isotope data are from Chen et al. (2022).

Because radiogenic Sr–Pb–Nd–Hf isotope compositions are very different among subducting slab lithologies and mantle wedge peridotite, and incompatible trace elements Sr, Pb, Nd, and Hf with quite different mobility during slab dehydration/partial melting (e.g., Herman and Rubatto, 2009; Johnson and Plank, 2000; Kessel et al., 2005; Klimm et al., 2008), they are documented to be ideal tracers for material transportation from slab to arc magma sources in subduction zones (e.g., Elliott, 2003; Elliott et al., 1997; Hawkesworth et al., 1997; Miller et al.,

1994; Straub and Zellmer, 2012; Straub et al., 2015; White, 2015; Zheng, 2019). For this reason, correlations between δ^{56}Fe or δ^{26}Mg values and these tracers of recycled crustal components are expected to provide the most convincing evidence for the controlling effect of crustal recycling in dictating the Mg and Fe isotope variations of arc rocks (e.g., Foden et al., 2018; Hu et al., 2020). Nevertheless, different from radiogenic Sr–Pb–Nd–Hf isotopes that remain unchanged during partial melting and fractional crystallization, Mg and Fe isotopes can be fractionated to different extents during these processes (Dauphas et al., 2017; Teng et al., 2017). Furthermore, crustal contamination or magma mixing in the overlying crust would also change both the Fe–Mg and radiogenic isotope compositions of arc rocks. Therefore, before we use the above covariant relationships to trace crustal recycling and other processes during arc magmatism in the Neo-Tethys oceanic subduction zones, the potential influences of fractional crystallization, crustal contamination, and magma mixing should be carefully evaluated.

5.2 Fractional crystallization, crustal assimilation, and magma mixing

The most robust evidence for magma mixing or crustal contamination is the disequilibrium petrological textures or mineral structures/compositions, and covariation between differentiation indices (e.g., MgO, Mg#, SiO_2) and radiogenic isotopes or highly incompatible trace element ratios/contents (e.g., DePaolo, 1981; Gill, 1981). However, the previous studies documented that both kinds of evidence are lacking for the investigated Gangdese arc rocks (e.g., Chen et al., 2022; Ma et al., 2013b; Ma et al., 2013c; Xu et al., 2015; Yin et al., 2020; Zheng et al., 2014;). In addition, there is no covariation between Sr concentration and $(^{87}Sr/^{86}Sr)_i$ ratio (Fig. S1a in Appendix B), Nd concentration and $\varepsilon_{Nd}(t)$ value (Fig. S1b in Appendix B), Ce/Pb ratio and $(^{206}Pb/^{204}Pb)_i$ ratio (Fig. S1c in Appendix B), Nb/U ratio and $\varepsilon_{Hf}(t)$ value (Fig. S1d in Appendix B), which further excluded the significant influence of crustal contamination on the geochemical features of these rocks. As an exception, Ma et al. (2013a) proposed that the composition of an outlier, a diorite sample from the Zhengga pluton with Sr and Nd isotope compositions that are much more enriched than the rest of Gangdese arc rocks, may have been formed by assimilation of a large amount (~30 wt.%) of upper crustal materials (gneiss) into mantle-derived magmas. Nevertheless, recently, Chen et al. (2022) demonstrated that new sampling and analyses revealed that this sample is not an outlier. This sample and other samples from the same pluton show close Sr–Pb–Nd–Hf isotope affinity with the local subducting sediments, demonstrating clearly that recycled sediments in their sources rather than assimilation of an unrealistic large amount of cold upper crust have dictated their radiogenic isotope compositions.

Most of the investigated arc rocks exhibit low Mg# values (< 60) and Ni concentrations (< 50 ppm), except for some samples from the EGA (Chen et al., 2022). Such geochemical features cannot be the primary features of depleted mantle-derived melts (Schmidt and Jagoutz, 2017), but indicate fractional crystallization of Mg-rich minerals from primary mantle melts (Müntener and Ulmer, 2018). In general, the whole-rock Mg isotopic compositions remain largely unchanged during the differentiation of basaltic magma (Teng et al. 2007, 2010). However, magmatic differentiation involving spinel with heavy Mg isotope and garnet with light Mg isotope could potentially cause Mg isotope fractionation (e.g., Su et al., 2019; Wang, S. J. et al., 2016). As shown in Fig. 5, the δ^{26}Mg values of these plutonic rocks do not correlate with their Cr contents or Dy/Yb ratios—chemical indices of chromite or garnet crystallization—indicating that fractional crystallization of neither Yb-rich garnet with light Mg isotope nor Cr-rich spinel with a heavy isotope, from the magmas, could be responsible for the variable δ^{26}Mg

values of these arc rocks. The lack of covariation between Mg isotope and MgO contents (Fig. 2A) also argues against the significant influence of fractional crystallization on the Mg isotope composition of these rocks.

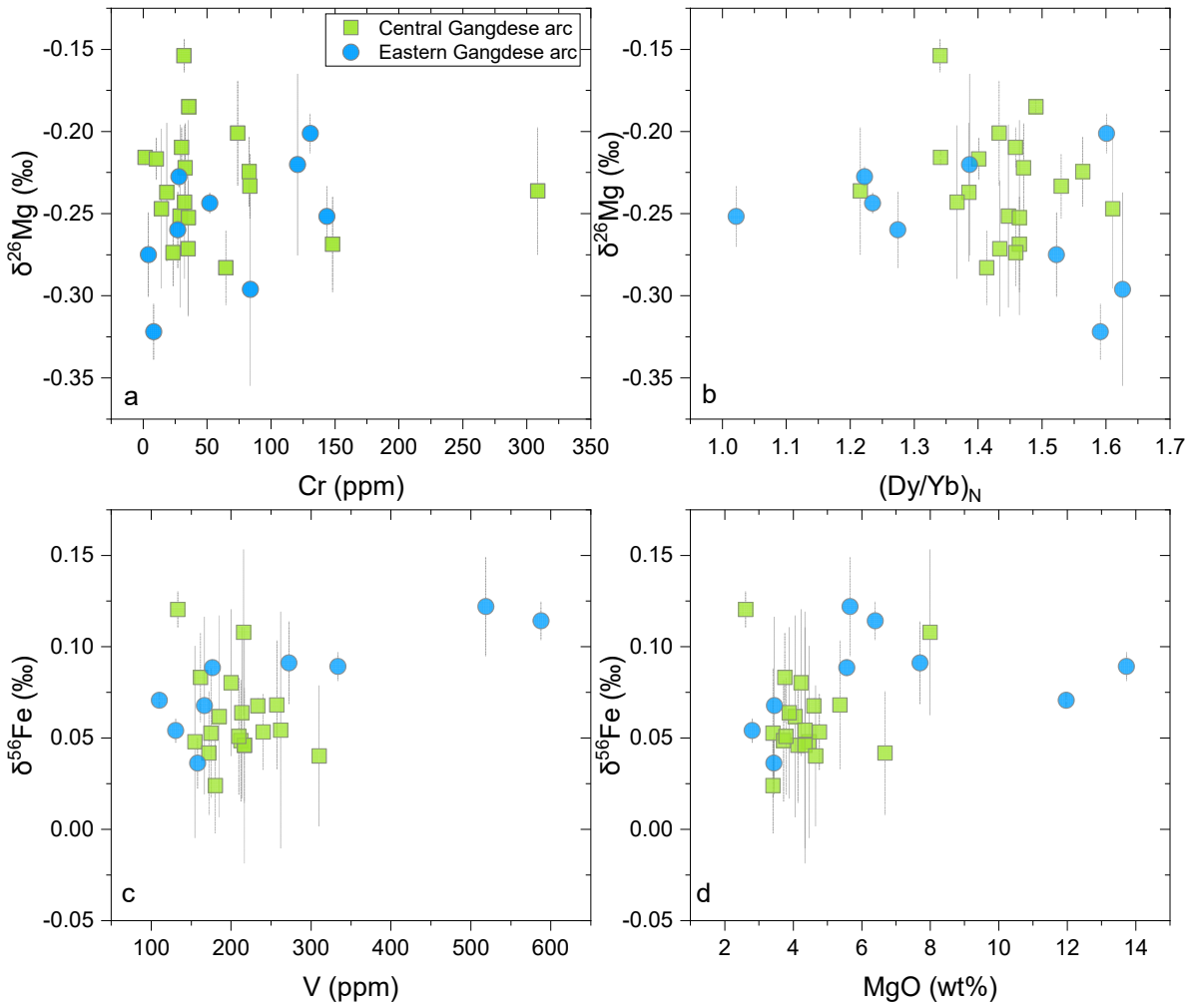

Figure 5. Fe–Mg isotope compositions in comparison with magma differentiation indices for the Gangdese arc rocks. (a) δ^{26}Mg vs. *Cr*; (b) δ^{26}Mg vs. $(Dy/Yb)_N$; (c) δ^{56}Fe vs. *V*; (d) δ^{56}Fe vs. MgO. The major-trace element data are from Chen et al. (2022). Note that the lack of covariation between Fe–Mg isotopes and differentiation indices suggests that fractional crystallization of garnet, magnetite, and other Fe–Mg- bearing minerals did not dominate the Fe–Mg isotope variation of the Gangdese arc rocks.

The potential role of fractional crystallization in modifying the Fe isotopic composition of mafic magmas has been intensively discussed and modeled (e.g., Foden et al., 2018; Schuessler et al., 2009; Sossi et al., 2012; Teng et al., 2008; Wawryk and Foden, 2017). Among common rock-forming or accessory Fe-bearing minerals in mafic rocks, magnetite stands out, for it tends to have heavier, while other minerals such as olivine and pyroxenes have lighter, Fe

isotopes than equilibrium melts (e.g., Sossi et al., 2012). It's clear that magnetite crystallizing alone would decrease the δ^{56}Fe values of the differentiating melt (Foden et al., 2018). Nevertheless, although magnetite crystallization would be promoted in the oxidized arc magmas (e.g., Feig et al., 2010), its emergence was usually preceded by a time interval of olivine ± pyroxene crystallization (Dauphas et al., 2017). The co-precipitation of magnetite with iron-magnesite silicate would still result in slight heavy iron isotope enrichment (Dauphas et al., 2017). There is no covariation between δ^{56}Fe values and V (Fe, Ti, not shown) or MgO contents (Figs. 5C and 5D)—chemical indices of magnetite or olivine ± pyroxene crystallization—indicating that fractional crystallization of neither magnetite nor olivine ± pyroxene can account for the variably low δ^{56}Fe values of these arc rocks. Therefore, fractional crystallization cannot explain the consistently lighter Fe isotope compositions of the Gangdese arc rocks than MORB (Fig. 2).

In summary, magma mixing, and fractional crystallization with or without crustal contamination do not significantly change the Fe–Mg isotopes of the Gangdese arc mafic rocks. On the other hand, the variable δ^{26}Mg and lighter- than-MORB δ^{56}Fe values of the mafic arc rocks should primarily have originated from their magma sources, similar to their enriched incompatible trace elements and radiogenic Sr–Pb–Nd–Hf isotope compositions (Chen et al., 2022).

5.3 Fe–Mg isotope variation of the EGA and sediment recycling

The Gangdese arc rocks with variably enriched Sr–Pb–Nd–Hf isotopic compositions have δ^{56}Fe values that are situated between MORB and mantle peridotite values (Fig. 2). Previous studies proposed that the lighter than MORB Fe isotope composition of arc rocks must either have resulted from the extraction of melts with heavy Fe isotope from the peridotite sources, or been produced by incorporation of slab materials with light Fe isotope composition into their magma sources, or a combination of both, but the relative contribution of the two factors is debated (e.g., Dauphas et al., 2009, 2017; Deng et al., 2022; Foden et al., 2018; Nebel et al., 2015). While melt extraction would lead to the depletion of the mantle residual in heavy Fe isotopes (Weyer and Ionov, 2007), the slab contribution is hard to evaluate. The subducting lithology is highly variable in Fe isotopes and so far, no clear covariation between robust geochemical tracers of slab components and Fe isotopes has been found to undisputedly constraint the direction of mantle wedge Fe isotopes shifting in response to slab metasomatism (Deng et al., 2022; Foden et al., 2018; Nebel et al., 2015).

Given the quite good covariations between Fe isotopes and radiogenic isotopes (Fig. 4) for EGA rocks, source mixing between the mantle and isotope enriched end-member with relatively heavy Fe isotope composition rather than different extents of mantle depletion would have dominated the Fe isotope variation of these rocks. This is because although a lower degree of mantle melting would possibly produce melts with heavier Fe isotope composition (Weyer and Ionov, 2007), it can't result in different radiogenic isotope compositions in the melts. It is easy to connect this Fe isotope heavy slab end-member to sediment, because sediment is the only candidate that occupies highly enriched Sr–Pb–Nd–Hf isotope compositions. More importantly, our analyzed local trench sediments not only have Sr–Pb–Nd–Hf isotope compositions that are enriched enough to cover the isotope variation of these arc rocks (Chen et al., 2022), but also have Fe isotope compositions that are heavy enough to encompass all the arc rocks (Fig. 6). Our inferred source mixing model got support from the good negative covariation between δ^{56}Fe

values and Zr/Hf ratios (Fig. 7b) as sediment-derived melts are quite lower in Zr/Hf ratios due to the residue of zircon (e.g., Hermann and Rubatto, 2009) than mantle peridotite (~3 vs. ~40), although the sediments themselves commonly show Zr/Hf ratios comparable to the mantle (e.g., Plank, 2014; Salters and Stracke, 2004). Therefore, it is likely, that recycling sediment-derived melts to the arc magma sources can readily explain the observed covariation patterns between Fe isotope and radiogenic isotope, as well as trace element ratios in EGA rocks, at least in a qualitative sense.

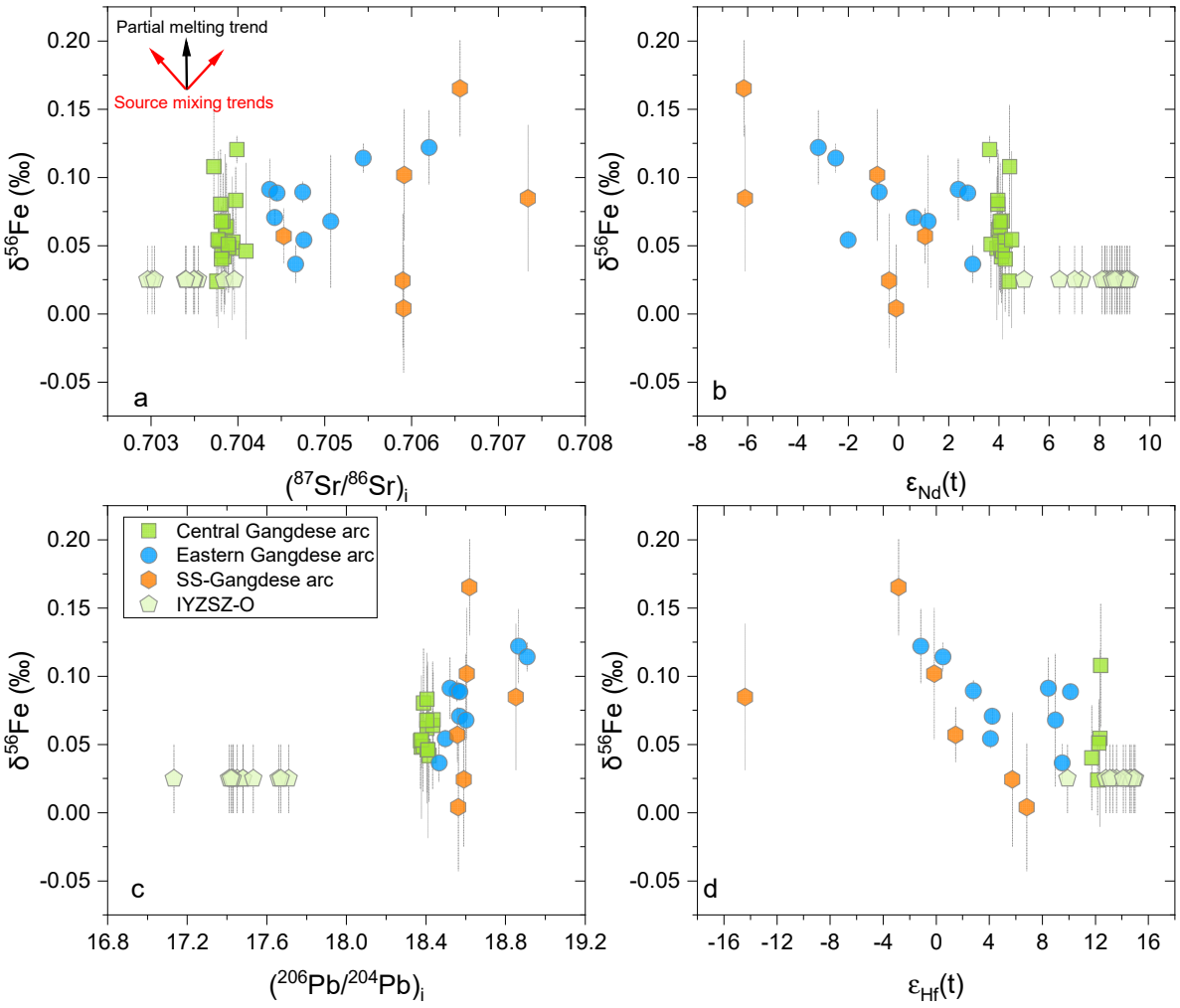

Figure 6. Fe isotope composition in comparison with Sr–Pb–Nd–Hf isotopes for the Gangdese arc rocks, Gangdese arc trench sediments, as well as IYZSZ ophiolites. (a) δ^{56}Fe vs. $(^{87}Sr/^{86}Sr)_i$; (b) δ^{56}Fe vs. $\varepsilon_{Nd}(t)$; (c) δ^{56}Fe vs. $(^{206}Pb/^{204}Pb)_i$; (d) δ^{56}Fe vs. $\varepsilon_{Hf}(t)$. The Mg and Fe isotope compositions for mantle peridotite from IYZSZ ophiolites are assigned as the same as normal mantle peridotite of Craddock et al. (2013) and Teng et al. (2010), respectively; The Sr–Pb–Nd–Hf isotope data for arc rocks and sediments are from Chen et al. (2022), and for IYZSZ ophiolites are from Xu and Castillo (2004), Zhang et al. (2005), and Zhang et al. (2016).

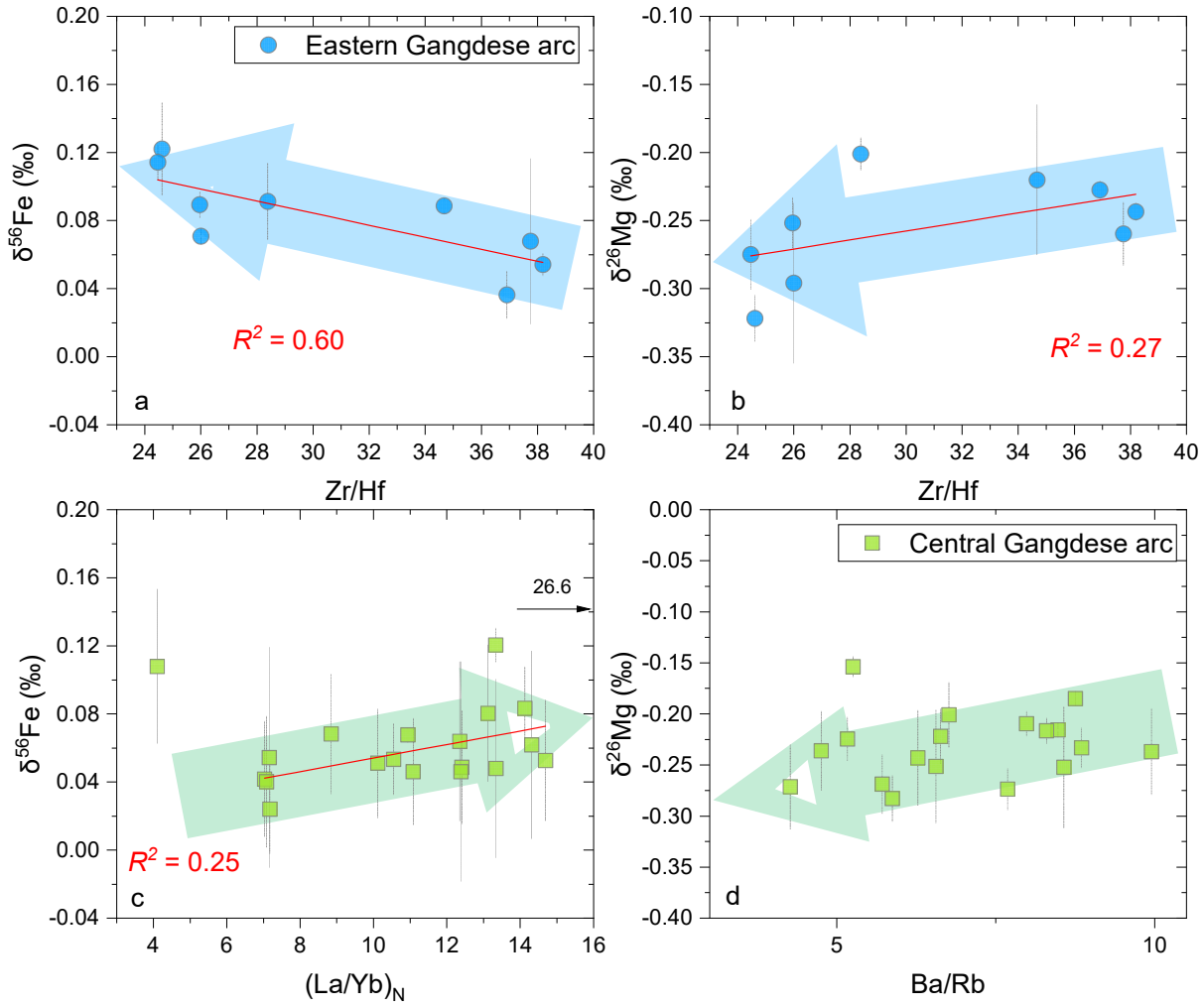

Figure 7. Fe–Mg isotope compositions in comparison with selective major and incompatible trace element ratios for the Gangdese arc rocks. (a) δ^{56}Fe vs. Zr/Hf; (b) δ^{26}Mg vs. Zr/Hf; (c) δ^{56}Fe vs. $(La/Yb)_N$; (d) δ^{26}Mg vs. Ba/Rb. The major-trace element data are from Chen et al. (2022).

To test this interpretation, we carried out binary mixing modeling between mantle peridotite and bulk sediments or sediment-derived melts (Table A1 in Appendix A); the modeling results are illustrated in Fig. 8. Mixing between mantle peridotite and bulk sediments generates values that decrease δ^{56}Fe with minimal change in $\varepsilon_{Nd}(t)$ of the melts, these values are inconsistent with measured values for EGA rocks (Figs. 8a and 8c). On the other hand, the observed mixing trends between mantle peridotite and sediment-derived melts passed nearly all the EGA rocks including some CGA rocks with relatively low δ^{56}Fe values (Figs. 8b and 8d). These quantitative results confirm the inference that the recycling of trench sediments to the magma sources in the form of melts resulted in the covariation between δ^{56}Fe and $\varepsilon_{Nd}(t)$ of the EGA rocks.

In this regard, our results suggest that even though the added slab components are heavy in Fe isotopes, it still can't buffer the effect of arc mantle depletion in leading the arc magma Fe

isotopes to light values. This supports the idea that the relatively light Fe isotope compositions of arc rocks most likely resulted from repeated fluid-fluxed melting of the subarc mantle (Foden et al., 2018).

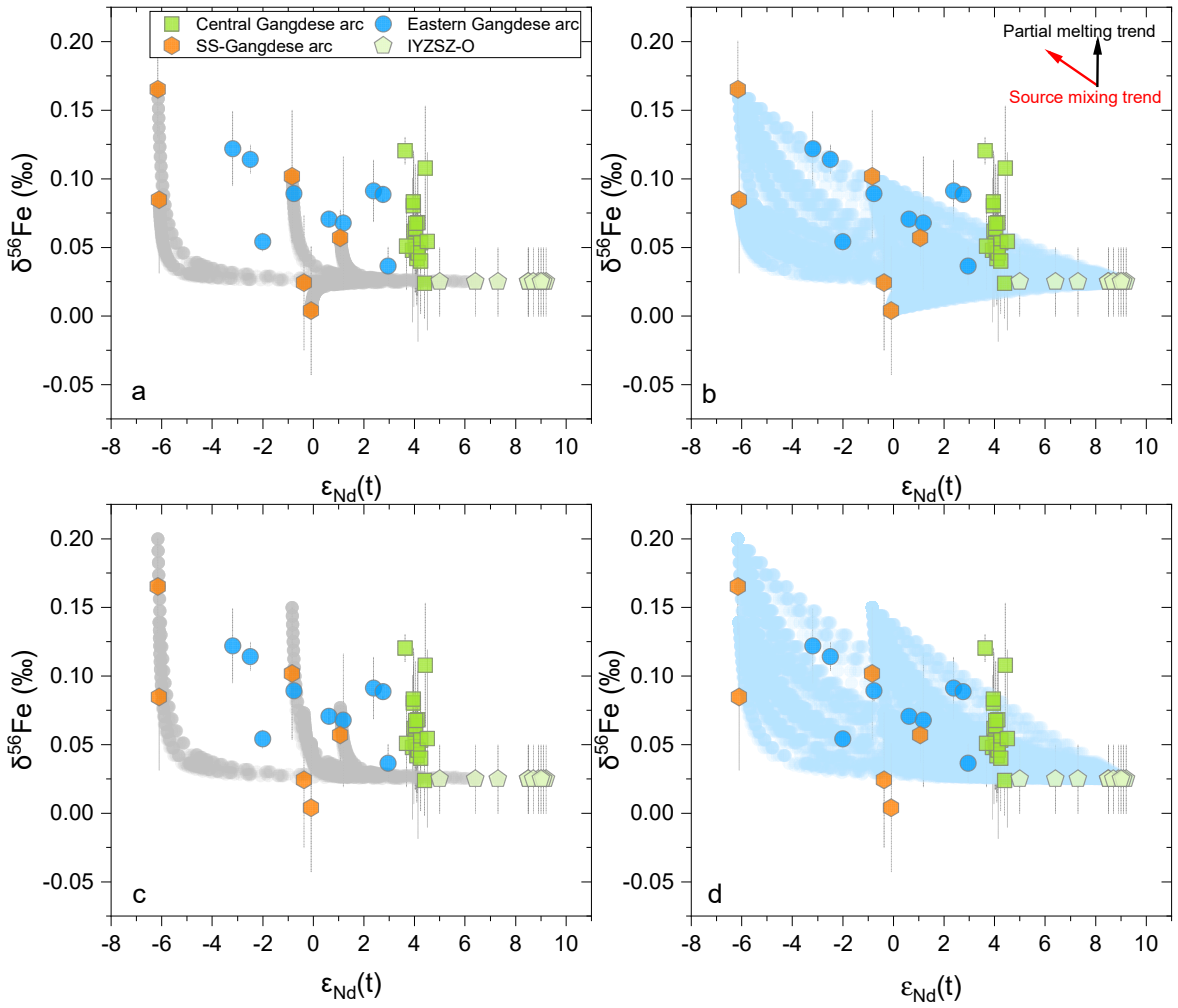

Figure 8. δ^{56}Fe versus $\varepsilon_{Nd}(t)$ plots showing the results of binary mixing modeling between depleted mantle wedge peridotite and bulk Gangdese arc trench sediments (a and c), or sediment-derived melts (b and d) for the Fe and Nd isotope compositions of the EGA rocks. Modeling parameters are listed in Table A1. Data sources for the bulk sediments and depleted mantle peridotite are the same as those in Fig. 6. The composition of sediment-derived melts is calculated from the Gangdese arc sediments and the bulk partition coefficients between sediment protoliths and melts reported by Hermann and Rubatto (2009). Both the reported δ^{56}Fe value (a and b) and the reported δ^{56}Fe value plus 2σ (c and d) for each sediment sample were used in the modeling. Noteworthy is that sediment-derived melts, especially when reported values plus 2σ were used (d), mixing with depleted mantle peridotite can readily reproduce the δ^{56}Fe and $\varepsilon_{Nd}(t)$ values of the EGA rocks while bulk sediments cannot.

The Mg isotope composition of the EGA rocks is comparable to MORB with restricted variation (Fig. 2), like the lavas from the Costa Rica and Kamchatka arcs (Li, S. G., et al., 2017). Nevertheless, it also shows good covariation with Sr–Pb–Nd–Hf isotopes (Fig. 3). Because Mg isotope composition does not change much during mantle melting unless large amounts of garnet or spinel are involved (Su et al., 2019; Wang, S. J. et al., 2016), which is not the case for these rocks (Fig. 5), and mantle melting does not lead to radiogenic isotope fractionation between melts and solid residual, the observed covariations can only be produced by source mixing. The required sediment end-member should have lighter Mg isotope composition than mantle peridotite, which is consistent with the composition of the analyzed trench sediments (Figs. 2 and 9). Therefore, from a qualitative point of view, the recycling of sediments themselves or melts derived from them to the arc magma sources can explain the observed covariations (Fig. 9). Our inferred source mixing model got support from the roughly positive covariation between δ^{26}Mg values and Zr/Hf ratios for the majority of the EGA samples (Fig. 7b) because sediment-derived melts are the only candidate that has low enough Zr/Hf ratios to meet the requirement for the light Mg isotope end-member with enriched radiogenic isotopes (Figs 3 and 7b). Like the case for Fe–Nd isotopes, results of quantitative modeling suggest that binary mixing between mantle peridotite and sediment-derived melts rather than bulk sediments can reproduce the Mg and Nd isotope compositions of the majority of EGA rocks (Fig. 10).

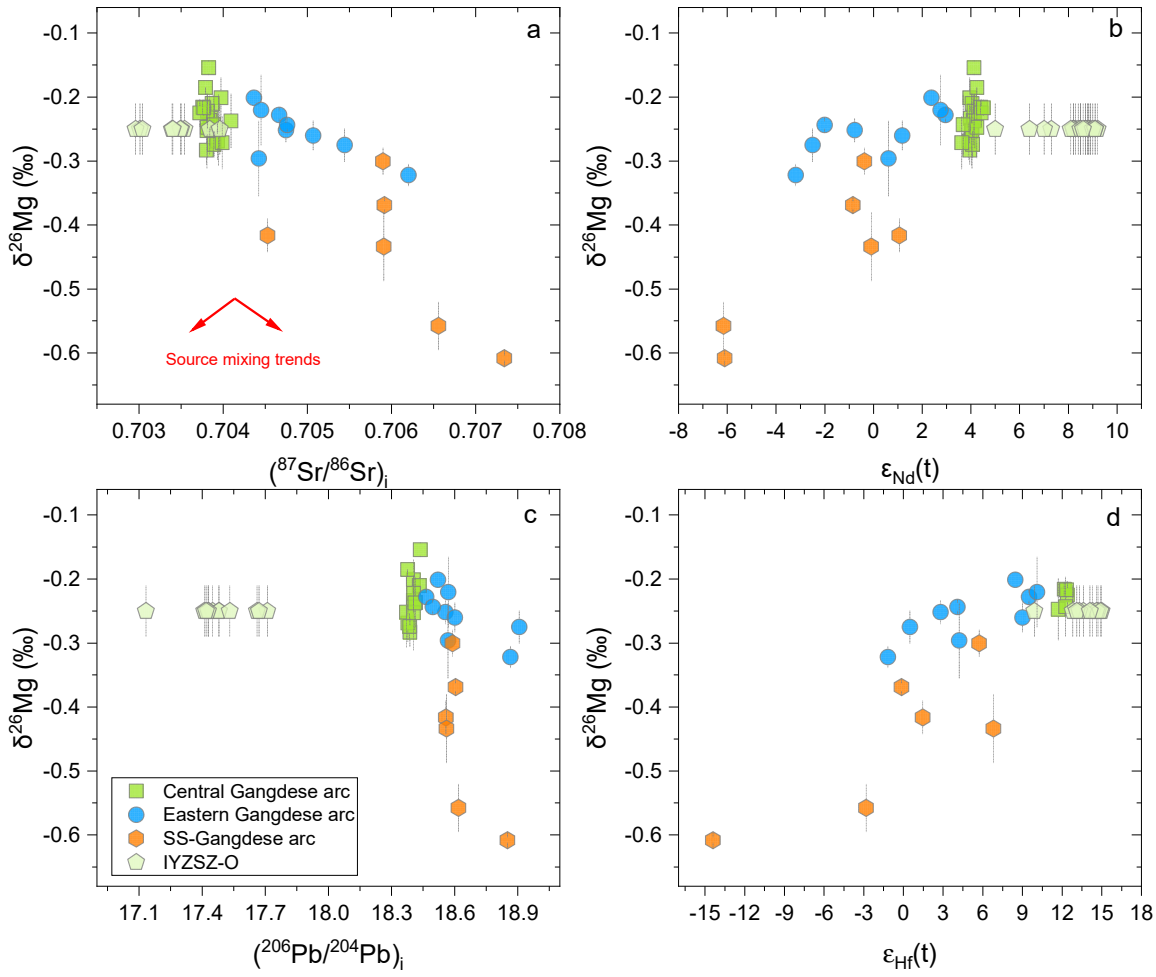

Figure 9. Mg isotope composition in comparison with Sr–Pb–Nd–Hf isotopes for the Gangdese arc rocks, Gangdese arc trench sediments, as well as IYZSZ ophiolites. (a) δ^{26}Mg vs. $(^{87}Sr/^{86}Sr)_i$; (b) δ^{26}Mg vs. $\varepsilon_{Nd}(t)$; (c) δ^{26}Mg vs. $(^{206}Pb/^{204}Pb)_i$; (d) δ^{26}Mg vs. $\varepsilon_{Hf}(t)$. Data sources for the bulk sediments and depleted mantle peridotite are the same as those in Fig. 6. The Mg isotope compositions for mantle peridotite from IYZSZ ophiolites are assigned as the same to normal mantle peridotite of Teng et al. (2010).

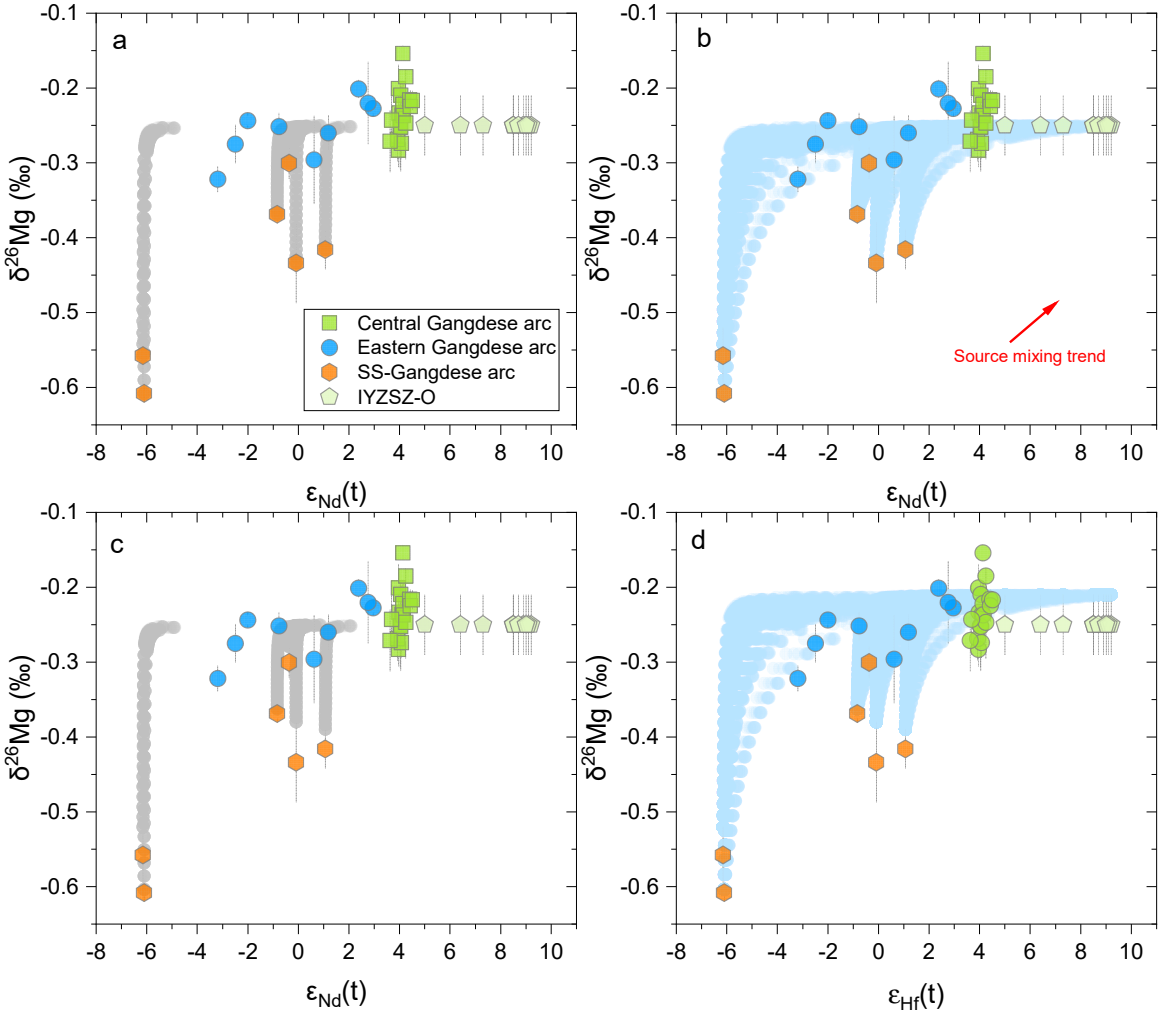

Figure 10. δ^{26}Mg versus $\varepsilon_{Nd}(t)$ plots showing the results of binary mixing modeling between depleted mantle wedge peridotite and bulk Gangdese arc trench sediments (a and c), or sediment–derived melts (b and d) for the Mg and Nd isotope compositions of the EGA rocks. Modeling parameters are listed in Table A1. Data sources for the bulk sediments and depleted mantle peridotite are the same as those in Fig. 9. The compositions of the sediment–derived melts are calculated from the Gangdese arc sediments and the bulk partition coefficients between sediment protoliths and melts reported by Hermann and Rubatto (2009). Both mixing between the reported δ^{26}Mg value (a and b) for each sediment sample and the recommended average

value for the depleted mantle peridotite, and between the reported value plus 2σ (c and d) for each sediment sample and the recommended average value plus 2σ for depleted mantle peridotite were used in the modeling. Consistent with the result of Fe–Nd isotope modeling, mixing between sediment-derived melts and depleted mantle peridotite, especially when reported values plus 2σ were used (d), can readily reproduce the δ^{26}Mg and $\varepsilon_{Nd}(t)$ values of the EGA rocks while bulk sediments cannot.

We noticed that sediment recycling was disputed in explaining the Mg and Fe isotopes variation of arc rocks by many previous studies (e.g., Foden et al., 2018; Hu et al., 2020; Nebel et al., 2015; Teng et al., 2016). Nebel et al. (2015) observed that there is no covariation between Fe isotope and radiogenic isotope tracers in mafic arc rocks from the Banda arc, Indonesia—a well-known arc for a prominent subducted sediment contribution to arc magma genesis. The authors, therefore, concluded that subducted sediment recycling would not cause resolvable Fe isotope variation of arc rocks, likely because of the low Fe content of the sediment-derived components. Foden et al. (2018) also could not find the expected covariant relationships between Fe isotope and radiogenic isotope compositions in arc rocks, even though a much larger dataset for global arc lavas was investigated. Teng et al. (2016) excluded sediment recycling as the origin of the heavy Mg isotope composition of the Lesser Antilles arc rocks because the δ^{26}Mg compositions of the local subducting sediments are not heavy enough (Hu et al., 2020; Teng et al., 2016), and because there is lack of covariation between Mg isotope and radiogenic isotope compositions for arc rocks from an arc that is well known for sediment recycling (e.g., Carpentier et al., 2008; Labanieh et al., 2010, 2012; Tang et al., 2014). However, similar to the trace elements and radiogenic isotopes (Plank, 2014), the Mg and Fe isotope composition of subducting sediments vary dramatically from trench to trench (Hu et al., 2017; Nebel et al., 2015; this study). In our case, the Gangdese trench sediments have consistently lighter Mg isotope composition than arc rocks and mantle peridotite with restricted variation, in contrast to the large range of Mg isotope composition for sediments from the Lesser Antilles arc, which are both lighter and heavier than the arc rocks and mantle peridotite (Teng et al., 2016). In addition, the Mg isotope variation of Gangdese arc rocks is restricted and comparable to normal mantle peridotite, as well as metasomatized arc mantle wedge (Hu et al., 2020), which means that we do not need to change the δ^{26}Mg values of the metasomatized mantle very much to produce the observed covariation patterns (Fig. 3). A similar argument would also work for Fe isotopes (Fig. 2B).

Different from these previous studies, we observed very well-presented covariant relationships between both Mg and Fe isotopes and radiogenic Sr–Pb–Nd–Hf isotopes for the Gangdese arc rocks that can readily be reproduced by source mixing between subducted local trench sediments-derived melts and the ambient mantle (Figs. 3, 4, 8 and 10). Therefore, we attributed the difference between our conclusion and those of previous studies which found the impact of sedimentary material invisible from the Fe–Mg isotope perspectives in arc magmas (e.g., Foden et al., 2018; Nebel et al., 2015; Teng et al., 2016), to mainly the different Fe–Mg isotopes and associated radiogenic isotopes as well as trace element compositions in the subducting sediments. All these differences make the detectable covariant relationships between Fe–Mg isotope compositions and Sr–Pb–Nd–Hf isotopes in our samples indetectable in their samples though the absolute deviations of the Fe–Mg isotope compositions of arc rocks from the mantle compositions may be comparable in our samples and their samples (Fig. 2).

As such, the present study provides solid evidence for the contribution of recycled sediment-derived melts in modifying the Fe and Mg isotope compositions of arc rock though the absolute extent of modification may be quite limited due to their much lower Fe, and especially Mg contents compared to mantle wedge peridotite.

5.4 Fe–Mg isotope variation of the CGA, serpentinite recycling, and mantle melting

In contrast to the EGA rocks, CGA rocks do not show good covariation between Fe–Mg and Sr–Pb–Nd–Hf isotope compositions. On the other hand, the Mg and Fe isotopes of the CGA samples stretch out straight from the end-members with relatively heavy Mg isotope, light Fe isotope, and less enriched Sr–Pb–Nd–Hf isotope to the lighter Mg and heavier Fe isotopes without obvious change in Sr–Pb–Nd–Hf isotope compositions (Figs. 3 and 4). Since a slab component including sediments is necessary to interpret the enriched Sr–Pb–Nd–Hf isotope compositions and characteristic trace element distribution patterns of the CGA rocks (Chen et al., 2022), the constant and relatively less enriched Sr–Pb–Nd–Hf isotope compositions of CGA rocks could be produced by source mixing between mantle peridotite and a consistent but relatively small amounts of sediment components, with or without variable amounts of AOC/serpentinite-derived components (Chen et al., 2022). This is because AOC/serpentinite-derived components would have much lower Sr, Nd, Pb, and Hf contents, as well as much closer Sr–Pb–Nd–Hf isotope compositions, compared to the mantle wedge than sediments (e.g., McCulloch et al., 1980; Spandler and Pirard, 2013; Staudigel, 2003, 2014), variation in their proportions, would have negligible influence on the Sr–Pb–Nd–Hf isotope compositions of the metasomatized mantle and arc rocks. The trends of increasing δ^{56}Fe values with consistent Sr–Pb–Nd–Hf isotopes can be attributed to decreasing extent of the metasomatized mantle melting, because of the preferential releasing of Fe^{3+} with heavy Fe isotope during low degree partial melting (e.g., Dauphas et al., 2009; Foden et al., 2018; Schauble, 2004; Weyer and Ionov, 2007). However, mantle sources with consistent amounts of sediment component cannot melt out magmas with quite different δ^{26}Mg values without the involvement of large amounts of garnet and/or spinel (Fig. 5; Wang, S. J. et al., 2016). Therefore, incorporation of various amounts of AOC/serpentinite-derived components in addition to sediment-derived components in the magma sources is necessary to explain the Mg isotope variation of the CGA rocks.

Although the absolute change of Fe isotope is not significant, the explanation that variation of the δ^{56}Fe values of the CGA samples corresponding to different extents of mantle melting got support from the roughly positive correlation between δ^{56}Fe values and $(La/Yb)_N$ ratios defined by all but one CGA samples (Fig. 7c), because the lower degree of source melting would lead to higher $(La/Yb)_N$ ratios in the melts. Further quantitative modeling on batch melting of the metasomatized mantle (Table A2 in Appendix A) did generally reproduce the observed covariation pattern in Fig. 7c (Fig. 11a). On the other hand, source mixing between different amounts of AOC/serpentinite-derived components with mantle peridotite in controlling the Mg isotope variation of the CGA samples got support from the roughly negative correlation between δ^{26}Mg values and Ba/Rb ratios (Fig. 7d), because while most subducted sediments, AOC, serpentinite, as well as sediment-derived melts have Ba/Rb > 10 (Herman and Rubatto, 2009; Plank, 2014; Spandler et al., 2014; Staudigel, 2003, 2014), AOC- or serpentinite-derived fluids are always characterized by Ba/Rb < 3 due to the much more soluble nature of Rb over Ba during dehydration (Kessel et al., 2005; Spandler et al., 2014). AOC has a wide δ^{26}Mg range with values ranging from much lighter to much heavier than the mantle peridotite (Teng et al., 2016, 2017), which would more or less fractionate during dehydration (Huang et al., 2020).

Nevertheless, AOC-derived fluid is documented to be too low in Mg to significantly change the Mg isotope composition of the metasomatized mantle (Hao et al., 2022; Hu et al., 2020; Liu et al., 2017). Serpentinite-derived fluids are documented to be much higher in MgO contents than AOC-derived fluids (Chen et al., 2016; Deschamps et al., 2013; Dvir et al., 2011; Scambelluri et al., 2014, 2015), and thus more efficient in modifying the Mg isotope composition of the metasomatized mantle and arc rocks (Hao et al., 2022; Hu et al., 2020; Teng et al., 2016; Zhao et al., 2023). Nevertheless, normal serpentinites are documented to be exclusively heavier in Mg isotopes than normal mantle due to weathering (Beinlich et al., 2014; Debret et al., 2016; Liu et al., 2017; Zhao et al., 2023). Moreover, although first-principles molecular dynamics simulations predict that equilibrium Mg isotope fractionation at low temperatures would cause aqueous fluids depleted in heavy Mg isotope compositions compared to lizardite (Wang, W. Z. et al., 2019), fluids released by high-temperature–high-pressure antigorite dehydration are demonstrated to be consistently heavier in Mg isotope than normal mantle (e.g., Chen et al., 2016; Hu et al., 2020; Teng et al., 2016). However, carbonated serpentinites can have δ^{26}Mg values as low as ~–0.7‰, and carbonation is ubiquitous for abyssal serpentinites (e.g., Beinlich et al., 2018; Oskierski et al. 2019). Therefore, carbonated serpentinite-derived fluids can serve as the potential low δ^{26}Mg-low Ba/Rb end-member in the magma sources of CGA rocks (Fig. 11b).

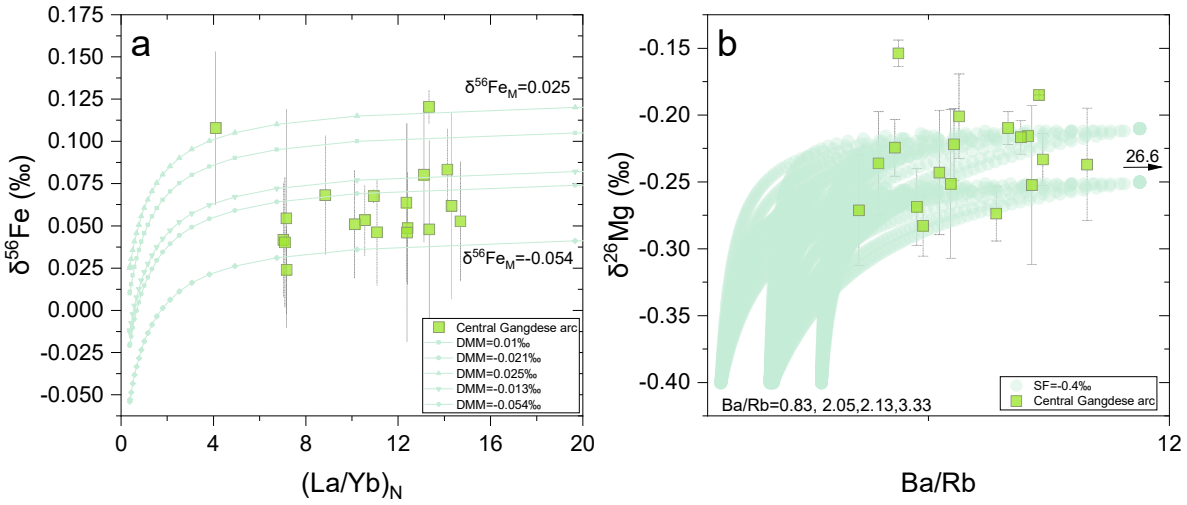

Figure 11. δ^{56}Fe versus $(La/Yb)_N$ (a) and δ^{26}Mg versus Ba/Rb (b) plots showing the results of mantle wedge peridotite batch melting and source mixing between subducting serpentinite-derived fluids and mantle wedge peridotite modeling, respectively. Modeling parameters are listed in Tables A2 and A3. The La, Yb, and Fe contents of the depleted mantle wedge are adopted from Workman and Hart (2005), and the $Fe3+/Fe_{Total}$ is adopted from Canil et al. (1994). The δ^{56}Fe value for the depleted mantle wedge peridotite and the isotope fractionation factor between the mantle and melt ($ln\alpha_{mantle\text{-}melt}$) are adopted from Weller and Ionov (2007). During partial melting, melt/solid partition coefficients for Fe^{2+} and Fe^{3+} are adopted from Canil et al. (1994), and melt/solid partition coefficients for La and Yb are adopted from Kessel et al. (2015). The Mg, Ba, and Rb contents for the serpentinite-derived fluid are from Scambelluri et al. (2015). The elemental composition of the depleted mantle wedge peridotite is from Workman and Hart (2005). The Mg isotope value for the carbonated serpentinite-derived fluid (SF) (δ^{26}Mg = –

639 0.40‰) is adopted from Beinlich et al. (2018) assuming negligible Mg isotope fractionation
640 during the dehydration of carbonated serpentinites. The results of the modeling would still be
641 true even though carbonated serpentinite dehydration releases aqueous fluid with a heavy Mg
642 isotope because we have chosen the highest value of the carbonated serpentinites reported by
643 Beinlich et al. (2018).

644 Quantitative modeling on binary mixing between carbonated serpentinite-derived fluids
645 (δ^{26}Mg = –0.40‰, see caption of Fig. 11 for the criterion of data selection) and mantle wedge
646 peridotite (Table A3 in Appendix A) obtained mixing trends passed nearly all the data points of
647 CGA samples (Fig. 11b). Therefore, source mixing between carbonated serpentinite-derived
648 fluids and mantle peridotite can readily explain the observed correlation between δ^{26}Mg values
649 and Ba/Rb ratios. Thus, different from previous studies which observed that serpentinite-derived
650 fluid recycling would lead to heavy Mg isotope composition of the arc magmas (Hao et al., 2022;
651 Hu et al., 2020; Teng et al., 2016; Zhao et al., 2023), the present study reveals that recycling of
652 carbonated serpentinite-derived fluid can also pull the Mg isotope values of the arc rocks in the
653 opposite direction, though not by much.

654 **6 Implications on processes of subduction zone crustal recycling**

655 The relative role of AOC-derived fluids plus sediment-derived melt, as well as
656 serpentinite-derived fluid, and diapiric solid mélange in transporting slab materials to the arc
657 magma sources to accomplish crustal recycling in subduction zones, has been a heated debate
658 recently (e.g., Chen et al., 2021; Codillo et al., 2018; Cruz-Uribe et al., 2018; Li, H. et al., 2022;
659 Nielsen and Marschall, 2017; Parolari et al., 2021; Turner and Langmuir, 2022).

660 Although mainly based on a new round of numerical modeling (e.g., Behn et al., 2011;
661 Marschall and Schumacher, 2012), an increasing number of geochemical and experimental
662 studies argue that mélange models have advantages over the traditional fluid/melt fluxed models
663 in explaining not only the major-trace elements, but also radiogenic isotope as well as
664 nontraditional stable isotope (e.g., Mg) compositions of individual arc rocks or global arc rocks
665 in general (e.g., Hao et al., 2022; Codillo et al., 2018; Cruz-Uribe et al., 2018; Nielsen and
666 Marschall, 2017; Parolari et al., 2021). On the other hand, considering that this model
667 intrinsically demands the low-pressure–high-temperature melting conditions for the oceanic crust
668 including sediments in the mélange or mélange-peridotite mixtures, and physical mixing of
669 sediments and oceanic crust with the mantle would significantly dilute the concentration of key
670 elements such as Ti and Zr in the mixtures, whether sufficient quantities of key accessory
671 minerals such as rutile and zircon will continue to stabilize during mélange melting to produce
672 the unique trace element geochemical characteristics of arc rocks was severely questioned (e.g.,
673 Li et al., 2022; Pirard and Hermann, 2015; Turner and Langmuir, 2022).

674 The present study observed strong covariation between Mg and Fe isotope compositions
675 with radiogenic isotopes (Figs. 3 and 4), which unequivocally demonstrated the controlling
676 effects of sediment recycling on both trace and major element isotopes of the arc magmas (Figs.
677 6 and 9). Further quantitative modeling indicates that the sediment components in the arc magma
678 sources should be sediment-derived melts rather than bulk sediments (Figs. 8 and 10). This is
679 consistent with the inferred low Zr/Hf ratios of the sediment end-members (Figs. 7a and 7b) that
680 demand the residual of a significant amount of zircon during high-pressure–low-temperature
681 metasediments melting (Hermann and Rubatto, 2009).

On the other hand, the well-defined positive covariation between Mg isotope and Ba/Rb ratios (Fig. 7d) asks for AOC or serpentinite-derived fluids recycling in controlling the Mg isotope and Ba/Rb variations in the Gangdese arc rocks. The quantitative simulation indicates that the required recycled materials should have high Mg contents, which would be derived from serpentinite instead of AOC (Fig. 11b). Meanwhile, the required recycled components should have a slightly light Mg isotope composition than normal mantle (Fig. 11b). The candidate material most likely to meet both requirements is the aqueous fluid released by dehydration of carbonated serpentinites, as it is characterized by a lighter Mg isotope composition than the normal mantle (e.g., Beinlich et al., 2018; Oskierski et al. 2019). Therefore, this observation again provides major element isotope evidence to argue against the significant role of bulk serpentinite in recycling slab materials to the Gangdese arc magmatism, as claimed by the mélange diapir model, but instead, provides evidence for the key role of carbonated serpentinite-derived fluids in subduction zone crustal recycling and arc magmatism.

As such, the present case study based mainly on the results of stable isotopes of Fe–Mg major elements provides further support to the idea that variable in-situ fractionated slab components (e.g., Ellam and Hawkesworth, 1988; Elliot, 2003; Elliot et al., 1997; Gill, 1981), rather than sub-solidus unfractionated bulk mélange composed of metasediments, AOC, and hydrated mantle peridotite (e.g., Codillo et al., 2018; Cruz-Uribe et al., 2018; Nielsen and Marschall, 2017), are the dominant agents for material transportation from slab to mantle wedge in oceanic subduction zones.

7 Conclusions

Well-defined covariations between Fe–Mg isotopes and radiogenic isotopes, as well as incompatible trace element ratios, were observed for the Gangdese arc mafic plutonic rocks, which combined with the Fe–Mg isotope compositions of the local subducting trench sediments, revealed a complex crustal recycling, slab-mantle reaction, as well as metasomatized mantle melting processes for the Cretaceous Gangdese arc magmatism and shed new light on subduction zone crustal recycling:

(1) Source mixing between subducting sediment-derived melts with relatively heavy Fe isotope, light Mg isotope, variously enriched Sr–Pb–Nd–Hf isotope, as well as low Zr/Hf ratios, and mantle wedge peridotite, dictated the variation of Fe–Mg isotopes and other geochemical features of the EGA rocks, though preceding melt extraction determined the lighter than MORB Fe isotope composition of these rocks. Although sediment-derived melts are much lower in Mg and Fe contents compared to the mantle wedge peridotite, their distinct Mg and Fe isotope compositions to the peridotite make their impact visible in mafic arc magmas, the subtle changes they cause on the Mg and Fe isotopes of arc rocks would be hard to identify unless they covary with conventional tracers.

(2) Mixing between carbonated serpentinite-derived fluids with relatively light Mg isotopes and high Mg contents as well as quite low Ba/Rb ratios with mantle wedge peridotite dictated the Mg and other geochemical features of the CGA rocks. Different from previous studies which found that serpentinite–derived fluid recycling would result in the heavy Mg isotopic composition in arc magmas, we found that such recycling would also shift Mg isotopic values of the arc rocks in the opposite direction, though the magnitude is limited.

(3) The results of stable isotopes of Fe–Mg major elements provide further support to the idea that variable in-situ fractionated slab components (fluids/melts) rather than sub-solidus unfractionated solid mélanges are the main material transporting agents from slab to mantle wedge.

Acknowledgments

This study was supported by funds from the National Natural Science Foundation of China (92058211, 92155306, 42072061), the Strategic Priority Research Program (B) of the Chinese Academy of Sciences (XDB41000000), and the Shandong Excellent Young Scientist Grant (ZR2022YQ32). We thank Dr. Yang Zhang for his help with Mg and Fe isotope analyses.

Data Availability Statement

The data for this paper are contained in the text, figures and supporting information, and are also available at Zenodo via https://doi.org/10.5281/zenodo.7758429.

References

An, W, Hu, X. M, & Garzanti, E (2018), Discovery of Upper Cretaceous Neo-Tethyan trench deposits in south Tibet (Luogangcuo Formation). *Lithosphere, 10*, 446–459. https://doi.org/10.1130/L690.1

Behn, M. D., Kelemen, P. B., Hirth, G., Hacker, B. R., & Massonne, H. J. (2011), Diapirs as the source of the sediment signature in arc lavas. *Nature Geoscience, 4*, 641-646. https://doi.org/10.1038/ngeo1214

Beinlich, A., Austrheim, H., Mavromatis, V., Grguric, B., Putnis, C. V., & Putnis, A. (2018), Peridotite weathering is the missing ingredient of Earth's continental crust composition. *Nature communications, 9*, 1-12. https://doi.org/10.1038/s41467-018-03039-9

Beinlich, A., Mavromatis, V., Austrheim, H., & Oelkers, E. H. (2014), Inter-mineral Mg isotope fractionation during hydrothermal ultramafic rock alteration–Implications for the global Mg-cycle. *Earth and Planetary Science Letters, 392*, 166-176. https://doi.org/10.1016/j.epsl.2014.02.028

Bindeman, I. (2008), Oxygen isotopes in mantle and crustal magmas as revealed by single crystal analysis. *Reviews in Mineralogy and Geochemistry, 69*, 445-478. https://doi.org/10.2138/rmg.2008.69.12

Canil, D., O'Neill, H. S. C., Pearson, D. G., Rudnick, R. L., McDonough, W. F., & Carswell, D. A. (1994), Ferric iron in peridotites and mantle oxidation states. *Earth and Planetary Science Letters, 123*, 205-220. https://doi.org/10.1016/0012-821X(94)90268-2

Carpentier, M., Chauvel, C., & Mattielli, N. (2008), Pb–Nd isotopic constraints on sedimentary input into the Lesser Antilles arc system. *Earth and Planetary Science Letters, 272*, 199-211. https://doi.org/10.1016/j.epsl.2008.04.036

Chen, L., Zheng, Y. F., Zhao, Z. F., An, W., & Hu, X. (2022), Continental crust recycling in ancient oceanic subduction zone: Geochemical insights from arc mafic rocks and paleo-trench sediments in southern Tibet. *Lithos, 414*, 106619. https://doi.org/10.1016/j.lithos.2022.106619

Chen, L., Zheng, Y.F., Xu, Z., & Zhao, Z.F. (2021), Generation of andesite through partial melting of basaltic metasomatites in the mantle wedge: Insight from quantitative study of Andean andesites. *Geoscience Frontiers, 12*, 101124. https://doi.org/10.1016/j.gsf.2020.12.005

Chen, Y. X., Schertl, H. P., Zheng, Y. F., Huang, F., Zhou, K., & Gong, Y. Z. (2016), Mg–O isotopes trace the origin of Mg-rich fluids in the deeply subducted continental crust of Western Alps. *Earth and Planetary Science Letters, 456*, 157-167. https://doi.org/10.1016/j.epsl.2016.09.010

Codillo, E. A., Le Roux, V., & Marschall, H. R. (2018), Arc-like magmas generated by mélange-peridotite interaction in the mantle wedge. *Nature communications, 9*, 1-11. https://doi.org/10.1038/s41467-018-05313-2

Craddock, P. R., Warren, J. M., & Dauphas, N. (2013), Abyssal peridotites reveal the near-chondritic Fe isotopic composition of the Earth. *Earth and Planetary Science Letters, 365*, 63-76. https://doi.org/10.1016/j.epsl.2013.01.011

Cruz-Uribe, A. M., Marschall, H. R., Gaetani, G. A., & Le Roux, V. (2018), Generation of alkaline magmas in subduction zones by partial melting of mélange diapirs—An experimental study. *Geology, 46*, 343-346. https://doi.org/10.1130/G39956.1

Dai, J. G., Wang, C. S., Stern, R. J., Yang, K., & Shen, J. (2021), Forearc magmatic evolution during subduction initiation: Insights from an Early Cretaceous Tibetan ophiolite and comparison with the Izu-Bonin-Mariana forearc. *Bulletin, 133*, 753-776. https://doi.org/10.1130/B35644.1

Dauphas, N., Craddock, P. R., Asimow, P. D., Bennett, V. C., Nutman, A. P., & Ohnenstetter, D. (2009), Iron isotopes may reveal the redox conditions of mantle melting from Archean to Present. *Earth and Planetary Science Letters, 288*, 255-267. https://doi.org/10.1016/j.epsl.2009.09.029

Dauphas, N., John, S. G., & Rouxel, O. (2017), Iron isotope systematics. *Reviews in Mineralogy and Geochemistry, 82*, 415-510. https://doi.org/10.2138/rmg.2017.82.11

Debret, B., Millet, M. A., Pons, M. L., Bouilhol, P., Inglis, E., & Williams, H. (2016), Isotopic evidence for iron mobility during subduction. *Geology, 44*, 215-218. https://doi.org/10.1130/G37565.1

Deng, J., He, Y., Zartman, R. E., Yang, X., & Sun, W. (2022), Large iron isotope fractionation during mantle wedge serpentinization: Implications for iron isotopes of arc magmas. *Earth and Planetary Science Letters, 583*, 117423. https://doi.org/10.1016/j.epsl.2022.117423

DePaolo, D. J. (1981), Trace element and isotopic effects of combined wallrock assimilation and fractional crystallization. *Earth and Planetary Science Letters, 53*, 189-202. https://doi.org/10.1016/0012-821X(81)90153-9

Deschamps, F., Godard, M., Guillot, S., & Hattori, K. (2013), Geochemistry of subduction zone serpentinites: A review. *Lithos, 178*, 96-127. https://doi.org/10.1016/j.lithos.2013.05.019

Dvir, O., Pettke, T., Fumagalli, P., & Kessel, R. (2011), Fluids in the peridotite–water system up to 6 GPa and 800 C: new experimental constrains on dehydration reactions. *Contributions to Mineralogy and Petrology, 161*, 829-844. https://doi.org/10.1007/s00410-010-0567-2

Eiler, J. M., Crawford, A., Elliott, T. I. M., Farley, K. A., Valley, J. W., & Stolper, E. M. (2000), Oxygen isotope geochemistry of oceanic-arc lavas. *Journal of Petrology, 41*, 229-256. https://doi.org/10.1093/petrology/41.2.229

El Korh A., Luais B., Deloule E., & Cividini D. (2017), Iron isotope fractionation in subduction-related high-pressure metabasites (Ile de Groix, France). *Contributions to Mineralogy and Petrology, 172*, 41. https://doi.org/10.1007/s00410-017-1357-x

Ellam, R., & Hawkesworth, C. J. (1988), Elemental and isotopic variations in subduction related basalts: Evidence for a three-component model. *Contributions to Mineralogy and Petrology, 98*, 72–80. https://doi.org/10.1007/BF00371911

Elliott, T. (2003), Tracers of the slab. *Geophysical Monograph-American Geophysical Union, 138*, 23-46. https://doi.org/10.1029/138GM03

Elliott, T., Plank, T., Zindler, A., White, W., & Bourdon, B. (1997), Element transport from slab to volcanic front at the Mariana arc. *Journal of Geophysical Research: Solid Earth, 102*, 14991-15019. https://doi.org/10.1029/97JB00788

Feig, S.T., Koepke, J., & Snow, J.E. (2010), Effect of oxygen fugacity and water on phase equilibria of a hydrous tholeiitic basalt. *Contributions to Mineralogy and Petrology, 160*, 551–568. https://doi.org/10.1007/s00410-010-0493-3

Foden, J., Sossi, P. A., & Nebel, O. (2018), Controls on the iron isotopic composition of global arc magmas. *Earth and Planetary Science Letters, 494*, 190-201. https://doi.org/10.1016/j.epsl.2018.04.039

Gao, T., Ke, S., Li, R., Meng, X. N., He, Y., Liu, C., et al. (2019), High-precision magnesium isotope analysis of geological and environmental reference materials by multiple-collector inductively coupled plasma mass spectrometry. *Rapid Communications in Mass Spectrometry, 33*, 767-777. https://doi.org/10.1002/rcm.8376

Gill, J.B., (1981), Orogenic Andesites and Plate Tectonics. *Springer-Verlag, New York,* 390 pp.

Guo L., Jagoutz O., Shinevar W. J., & Zhang H. F. (2020), Formation and composition of the Late Cretaceous Gangdese arc lower crust in southern Tibet. *Contributions to Mineralogy and Petrology, 175*, 1-26. https://doi.org/10.1007/s00410-020-01696-y

Hao, L. L., Nan, X. Y., Kerr, A. C., Li, S. Q., Wu, Y. B., Wang, H., & Huang, F. (2022), Mg-Ba-Sr-Nd isotopic evidence for a mélange origin of early Paleozoic arc magmatism. *Earth and Planetary Science Letters, 577*, 117263. https://doi.org/10.1016/j.epsl.2021.117263

Hawkesworth, C. J., Turner, S. P., McDermott, F., Peate, D. W., & van Calsteren, P. (1997), U–Th isotopes in arc magmas: Implications for element transfer from the subducted crust. *Science, 276,* 551–555. https://doi.org/10.1126/science.276.5312.551

He, Y., Ke, S., Teng, F. Z., Wang, T., Wu, H., Lu, Y., & Li, S. (2015), High-precision iron isotope analysis of geological reference materials by high-resolution MC-ICP-MS. *Geostandards and Geoanalytical Research, 39*, 341-356. https://doi.org/10.1111/j.1751-908X.2014.00304.x

Hermann, J., & Rubatto, D. (2009), Accessory phase control on the trace element signature of sediment melts in subduction zones. *Chemical Geology, 265*, 512-526. https://doi.org/10.1016/j.chemgeo.2009.05.018

Hu, X., An, W., Garzanti, E., & Liu, Q. (2020), Recognition of trench basins in collisional orogens: Insights from the Yarlung Zangbo suture zone in southern Tibet. *Science China Earth Sciences, 63*, 2017-2028. https://doi.org/10.1007/s11430-019-9687-x

Hu, X., Garzanti, E., Wang, J., Huang, W., An, W., & Webb, A. (2016), The timing of India-Asia collision onset–Facts, theories, controversies. *Earth-Science Reviews, 160*, 264-299. https://doi.org/10.1016/j.earscirev.2016.07.014

Hu, Y., Teng, F. Z., & Ionov, D. A. (2020), Magnesium isotopic composition of metasomatized upper sub-arc mantle and its implications to Mg cycling in subduction zones. *Geochimica et Cosmochimica Acta, 278*, 219-234. https://doi.org/10.1016/j.gca.2019.09.030

Hu, Y., Teng, F. Z., Plank, T., & Huang, K. J. (2017), Magnesium isotopic composition of subducting marine sediments. *Chemical Geology, 466*, 15-31. https://doi.org/10.1016/j.gca.2019.09.030

Huang, J., Guo, S., Jin, Q. Z., & Huang, F. (2020), Iron and magnesium isotopic compositions of subduction-zone fluids and implications for arc volcanism. *Geochimica et Cosmochimica Acta, 278*, 376-391. https://doi.org/10.1016/j.gca.2019.06.020

Huang, K. J., Teng, F. Z., Plank, T., Staudigel, H., Hu, Y., & Bao, Z. Y. (2018), Magnesium isotopic composition of altered oceanic crust and the global Mg cycle. *Geochimica et Cosmochimica Acta, 238*, 357-373. https://doi.org/10.1016/j.gca.2018.07.011

Inglis E. C., Debret B., Burton K. W., Millet M.-A., Pons M.-L., Dale C. W., et al. (2017), The behavior of iron and zinc stable isotopes accompanying the subduction of mafic oceanic crust: a case study from Western Alpine ophiolites. *Geochemistry, Geophysics, Geosystems, 18*, 2562–2579. https://doi.org/10.1002/2016GC006735

Ji W. Q., Wu F. Y., Chung S. L., Li J. X., & Liu C. Z. (2009), Zircon U–Pb geochronology and Hf isotopic constraints on petrogenesis of the Gangdese batholith, southern Tibet. *Chemical Geology, 262*, 229-245. https://doi.org/10.1016/j.chemgeo.2009.01.020

Johnson, M. C., & Plank, T. (2000), Dehydration and melting experiments constrain the fate of subducted sediments. *Geochemistry, Geophysics, Geosystems, 1*. https://doi.org/10.1029/1999GC000014

Klimm, K., Blundy, J. D., & Green, T. H. (2008), Trace element partitioning and accessory phase saturation during H2O-saturated melting of basalt with implications for subduction zone chemical fluxes. *Journal of Petrology, 49*, 523-553. https://doi.org/10.1093/petrology/egn001

Kessel, R., Schmidt, M. W., Ulmer, P., & Pettke, T. (2005), Trace element signature of subduction-zone fluids, melts and supercritical liquids at 120–180 km depth. *Nature, 437*, 724-727. https://doi.org/10.1038/nature03971

Labanieh, S., Chauvel, C., Germa, A., & Quidelleur, X. (2012), Martinique: a clear case for sediment melting & slab dehydration as a function of distance to the trench. *Journal of Petrology, 53*, 2441-2464. https://10.1093/petrology/egs055

Labanieh, S., Chauvel, C., Germa, A., Quidelleur, X., & Lewin, E. (2010), Isotopic hyperbolas constrain sources and processes under the Lesser Antilles arc. *Earth and Planetary Science Letters, 298*, 35-46. https://doi.org/10.1016/j.epsl.2010.07.018

Li W.-Y., Teng F.-Z., Wing B. A., & Xiao Y. (2014), Limited magnesium isotope fractionation during metamorphic dehydration in metapelites from the Onawa contact aureole, Maine. *Geochemistry, Geophysics, Geosystems,* https://doi.org/10.1002/20GC004992. https://doi.org/10.1002/2013GC004992

Li W.-Y., Teng F.-Z., Xiao Y., & Huang J. (2011), High-temperature inter-mineral magnesium isotope fractionation in eclogite from the Dabie orogen, China. *Earth and Planetary Science Letters, 304*, 224–230. https://doi.org/10.1016/j.epsl.2011.01.035

Li, D. Y., Xiao, Y. L., Li, W. Y., Zhu, X., Williams, H. M., & Li, Y. L. (2016), Iron isotopic systematics of UHP eclogites respond to oxidizing fluid during exhumation. *Journal of Metamorphic Geology, 34*, 987-997. https://doi.org/10.1111/jmg.12217

Li, H., Hermann, J., & Zhang, L. (2022), Melting of subducted slab dictates trace element recycling in global arcs. *Science Advances, 8*, eabh2166. https://doi.org/10.1126/sciadv.abh2166

Li, S. G., Yang, W., Ke, S., Meng, X., Tian, H., Xu, L., et al. (2017), Deep carbon cycles constrained by a large-scale mantle Mg isotope anomaly in eastern China. *National Science Review, 4*, 111-120. https://doi.org/10.1093/nsr/nww070

Liu, P. P., Teng, F. Z., Dick, H. J., Zhou, M. F., & Chung, S. L. (2017), Magnesium isotopic composition of the oceanic mantle and oceanic Mg cycling. *Geochimica et Cosmochimica Acta, 206*, 151-165. https://doi.org/10.1016/j.gca.2017.02.016

Long Chen. (2023). Mg and Fe isotopes and other geochemical data for Gangdese arc mafic plutonic rocks and trench sediments [Data set]. Zenodo. https://doi.org/10.5281/zenodo.7758429

Ma L., Wang Q., Li, Z. X., Wyman D.A., Jiang Z. Q., Yang J. H., et al. (2013a), Early Late Cretaceous (ca. 93 Ma), norites and hornblendites in the Milin area, eastern Gangdese: Lithosphere–asthenosphere interaction during slab roll-back and an insight into early Late Cretaceous (ca. 100–80Ma), magmatic "flare-up" in southern Lhasa (Tibet). *Lithos, 172*, 17–30. https://doi.org/10.1016/j.lithos.2013.03.007

Ma L., Wang Q., Wyman D. A., Jiang Z. Q., Yang, J. H., Li Q. L., et al. (2013b), Late Cretaceous crustal growth in the Gangdese area, southern Tibet: Petrological and Sr-Nd-Hf-O isotopic evidence from Zhengga diorite-gabbro. *Chemical Geology, 349*, 54–70. https://doi.org/10.1016/j.chemgeo.2013.04.005

Ma L., Wang Q., Wyman D. A., Li Z. X., Jiang Z. Q., Yang J. H., et al. (2013c), Late Cretaceous (100–89 Ma), magnesian charnockites with adakitic affinities in the Milin area, eastern Gangdese: Partial melting of subducted oceanic crust & implications for crustal growth in southern Tibet. *Lithos, 175*, 315–332. https://doi.org/10.1016/j.lithos.2013.04.006

Marschall, H. R., & Schumacher, J. C. (2012), Arc magmas sourced from mélange diapirs in subduction zones. *Nature Geoscience, 5*, 862-867. https://doi.org/10.1038/ngeo1634

McCulloch, M. T., Gregory, R. T., Wasserburg, G. J., & Taylor Jr, H. P. (1980), A neodymium, strontium, and oxygen isotopic study of the Cretaceous Samail Ophiolite and implications for the petrogenesis and seawater-hydrothermal alteration of oceanic crust. *Earth and Planetary Science Letters, 46*, 201-211. https://doi.org/10.1016/0012-821X(80)90006-0

Miller, D. M., Goldstein, S. L., & Langmuir, C. H. (1994), Cerium/lead and lead isotope ratios in arc magmas and the enrichment of lead in the continents. *Nature, 368*, 514-520. https://doi.org/10.1038/368514a0

Morris, J. D., Leeman, W. P., & Tera, F. (1990), The subducted component in island arc lavas: constraints from Be isotopes and B–Be systematics. *Nature, 344*, 31-36. https://doi.org/10.1038/344031a0

Müntener O., & Ulmer P. (2018), Arc crust formation and differentiation constrained by experimental petrology. *American Journal of Science, 318*, 64-89.

Nebel, O., Sossi, P. A., Bénard, A., Wille, M., Vroon, P. Z., & Arculus, R. J. (2015), Redox-variability and controls in subduction zones from an iron-isotope perspective. *Earth and Planetary Science Letters, 432*, 142-151. https://doi.org/10.2475/01.2018.04

Nebel, O., Vroon, P. Z., van Westrenen, W., Iizuka, T., & Davies, G. R. (2011), The effect of sediment recycling in subduction zones on the Hf isotope character of new arc crust, Banda arc, Indonesia. *Earth and Planetary Science Letters, 303*, 240-250. https://doi.org/10.1016/j.epsl.2010.12.053

Nielsen, S. G., & Marschall, H. R. (2017), Geochemical evidence for mélange melting in global arcs. *Science Advances, 3*, e1602402. https://doi.org/10.1126/sciadv.1602402

Oskierski, H. C., Beinlich, A., Mavromatis, V., Altarawneh, M., & Dlugogorski, B. Z. (2019), Mg isotope fractionation during continental weathering and low temperature carbonation of ultramafic rocks. *Geochimica et Cosmochimica Acta, 262*, 60-77. https://doi.org/10.1016/j.gca.2019.07.019

Parolari, M., Gómez-Tuena, A., Errázuriz-Henao, C. & Cavazos-Tovar, J. G. (2021), Orogenic andesites and their link to the continental rock cycle. *Lithos, 382*, 105958. https://doi.org/10.1016/j.lithos.2020.105958

Pearce, J. A., & Peate, D. W. (1995), Tectonic implications of the composition of volcanic arc magmas. *Annual review of Earth and planetary sciences, 23*, 251-286. https://orca.cardiff.ac.uk/id/eprint/8499

Pirard, C., & Hermann, J. (2015), Focused fluid transfer through the mantle above subduction zones. *Geology, 43*, 915-918. https://doi.org/10.1130/G37026.1

Plank T. (2014), The chemical composition of subducting sediments. *Treatise on Geochemistry, 4*, 607–629. https://10.1016/B978-0-08-095975-7.00319-3

Rapp, R. P., Shimizu, N., Norman, M. D., & Applegate, G. S. (1999), Reaction between slab-derived melts and peridotite in the mantle wedge: experimental constraints at 3.8 GPa. *Chemical Geology, 160*, 335-356. https://doi.org/10.1016/S0009-2541(99)00106-0

Rouxel O, Dobbek N, Ludden J, & Fouquet Y (2003), Iron isotope fractionation during oceanic crust alteration. *Chemical Geology, 202*,155-182. https://doi.org/10.1016/j.chemgeo.2003.08.011

Rüpke, L. H., Morgan, J. P., Hort, M., & Connolly, J. A. (2004), Serpentine and the subduction zone water cycle. *Earth and Planetary Science Letters, 223*, 17-34. https://doi.org/10.1016/j.epsl.2004.04.018

Salters, V. J., & Stracke, A. (2004), Composition of the depleted mantle. *Geochemistry, Geophysics, Geosystems, 5*. https://doi.org/10.1029/2003GC000597

Scambelluri, M., Pettke, T., & Cannaò, E. (2015), Fluid-related inclusions in Alpine high-pressure peridotite reveal trace element recycling during subduction-zone dehydration of serpentinized mantle (Cima di Gagnone, Swiss Alps). *Earth and Planetary Science Letters, 429*, 45-59. https://doi.org/10.1016/j.epsl.2015.07.060

Scambelluri, M., Pettke, T., Rampone, E., Godard, M., & Reusser, E. (2014), Petrology and trace element budgets of high-pressure peridotites indicate subduction dehydration of serpentinized mantle (Cima di Gagnone, Central Alps, Switzerland). *Journal of Petrology, 55*, 459-498. https://doi.org/10.1093/petrology/egt068

Schauble, E. A. (2004), Applying stable isotope fractionation theory to new systems. *Reviews in Mineralogy Geochemistry, 55*, 65-111. https://doi.org/10.2138/gsrmg.55.1.65

Schmidt M. W., & Jagoutz O. (2017), The global systematics of primitive arc melts. *Geochemistry, Geophysics, Geosystems, 18*, 2817-2854. https://doi.org/10.1002/2016GC006699

Schuessler, J. A., Schoenberg, R., & Sigmarsson, O. (2009), Iron and lithium isotope systematics of the Hekla volcano, Iceland—evidence for Fe isotope fractionation during magma differentiation. *Chemical Geology, 258*, 78-91. https://doi.org/10.1016/j.chemgeo.2008.06.021

Searle, M. P., Windley, B. F., Coward, M. P., Cooper, D. J. W., Rex, A. J., Rex, D., et al. (1987), The closing of Tethys and the tectonics of the Himalaya. *Geological Society of America Bulletin, 98*, 678-701. https://doi.org/10.1130/0016-7606(1987)98<678:TCOTAT>2.0.CO;2

Singh, A. K., Chung, S. L., & Somerville, I. (2022), Petrogenesis of mantle peridotites in Neo-Tethyan ophiolites from the Eastern Himalaya and Indo-Myanmar Orogenic Belt in the geo-tectonic framework of Southeast Asia. *Geological Journal, 57*. DOI: 10.1002/gj 4629. https://doi.org/10.1002/gj.4629

Skora, S., & Blundy, J. (2010), High-pressure hydrous phase relations of radiolarian clay and implications for the involvement of subducted sediment in arc magmatism. *Journal of Petrology, 51*, 2211-2243. https://doi.org/10.1093/petrology/egq054

Sossi, P. A., Foden, J. D., & Halverson, G. P. (2012), Redox-controlled iron isotope fractionation during magmatic differentiation: an example from the Red Hill intrusion, S. Tasmania. *Contributions to Mineralogy and Petrology, 164*, 757-772. https://doi.org/10.1007/s00410-012-0769-x

Spandler, C., & Pirard, C. (2013), Element recycling from subducting slabs to arc crust: A review. *Lithos, 170*, 208-223. https://doi.org/10.1016/j.lithos.2013.02.016

995 Spandler, C., Pettke, T., & Hermann, J. (2014), Experimental study of trace element release
996 during ultrahigh-pressure serpentinite dehydration. *Earth and Planetary Science Letters, 391*,
997 296-306. https://doi.org/10.1016/j.epsl.2014.02.010
998 Staudigel, H. (2003), Hydrothermal alteration processes in the oceanic crust. *Treatise on*
999 *Geochemistry, 3*, 511-535. https://10.1016/B0-08-043751-6/03032-2
1000 Staudigel, H. (2014), Chemical fluxes from hydrothermal alteration of the oceanic crust. *Treatise*
1001 *on Geochemistry, 4*, 583-606. https://doi.org/10.1016/B978-0-08-095975-7.00318-1
1002 Stern R. J. (2002), Subduction zones. *Reviews of Geophysics, 40*, 1012.
1003 https://doi.org/10.1029/2001RG000108
1004 Straub, S. M., & Zellmer, G. F. (2012), Volcanic arcs as archives of plate tectonic change.
1005 *Gondwana Research, 21*, 495-516. https://doi.org/10.1016/j.gr.2011.10.006
1006 Straub, S. M., Gomez-Tuena, A., Bindeman, I. N., Bolge, L. L., Brandl, P. A., Espinasa-Perena,
1007 R., & Zellmer, G. F. (2015), Crustal recycling by subduction erosion in the central Mexican
1008 Volcanic Belt. *Geochimica et Cosmochimica Acta, 166*, 29-52.
1009 https://doi.org/10.1016/j.gca.2015.06.001
1010 Su, B. X., Hu, Y., Teng, F. Z., Xiao, Y., Zhang, H. F., Sun, Y., et al. (2019), Light Mg isotopes
1011 in mantle-derived lavas caused by chromite crystallization, instead of carbonatite metasomatism.
1012 *Earth and Planetary Science Letters, 522*, 79-86. https://doi.org/10.1016/j.epsl.2019.06.016
1013 Tang, M., Rudnick, R. L., & Chauvel, C. (2014), Sedimentary input to the source of Lesser
1014 Antilles lavas: A Li perspective. *Geochimica et Cosmochimica Acta, 144*, 43-58.
1015 https://doi.org/10.1016/j.gca.2014.09.003
1016 Tatsumi, Y., D. L. Hamilton, & R. W. Nesbitt. (1986), Chemical characteristics of fluid phase
1017 released from a subducted lithosphere and origin of arc magmas: evidence from high-pressure
1018 experiments and natural rocks. *Journal of Volcanology and Geothermal Research, 29*, 293-309.
1019 Teng, F. Z. (2017), Magnesium isotope geochemistry. *Reviews in Mineralogy and Geochemistry,*
1020 *82*, 219-287. https://doi.org/10.1016/0377-0273(86)90049-1
1021 Teng, F. Z., Dauphas, N., & Helz, R. T. (2008), Iron isotope fractionation during magmatic
1022 differentiation in Kilauea Iki lava lake. *Science, 320*, 1620-1622.
1023 https://10.1126/science.1157166
1024 Teng, F. Z., Hu, Y., & Chauvel, C. (2016), Magnesium isotope geochemistry in arc volcanism.
1025 *Proceedings of the National Academy of Sciences, 113*, 7082-7087.
1026 https://doi.org/10.1073/pnas.1518456113
1027 Teng, F. Z., Li, W. Y., Ke, S., Marty, B., Dauphas, N., Huang, S. C., et al. (2010), Magnesium
1028 isotopic composition of the Earth and chondrites. *Geochimica et Cosmochimica Acta, 74*, 4150-
1029 4166. https://doi.org/10.1016/j.gca.2010.04.019
1030 Teng, F. Z., Wadhwa, M., & Helz, R. T. (2007), Investigation of magnesium isotope
1031 fractionation during basalt differentiation: implications for a chondritic composition of the
1032 terrestrial mantle. *Earth and Planetary Science Letters, 261*, 84-92.
1033 https://doi.org/10.1016/j.epsl.2007.06.004
1034 Turner, S. J., & Langmuir, C. H. (2022), An evaluation of five models of arc volcanism. *Journal*
1035 *of Petrology, 63*. https://doi.org/10.1093/petrology/egac010
1036 Wang S.-J., Teng F.-Z., Li S.-G., & Hong J.-A. (2014), Magnesium isotopic systematics of mafic
1037 rocks during continental subduction. *Geochimica et Cosmochimica Acta, 143*, 34–48.
1038 https://doi.org/10.1016/j.gca.2014.03.029

Wang, S. J., Teng, F. Z., & Scott, J. M. (2016), Tracing the origin of continental HIMU-like intraplate volcanism using magnesium isotope systematics. *Geochimica et Cosmochimica Acta, 185*, 78-87. https://doi.org/10.1016/j.gca.2016.01.007

Wang, W., Zhou, C., Liu, Y., Wu, Z., & Huang, F. (2019), Equilibrium Mg isotope fractionation among aqueous Mg2+, carbonates, brucite and lizardite: Insights from first-principles molecular dynamics simulations. *Geochimica et Cosmochimica Acta, 250*, 117-129. https://doi.org/10.1016/j.gca.2019.01.042

Wawryk, C. M., & Foden, J. D. (2017), Iron-isotope systematics from the Batu Hijau Cu-Au deposit, Sumbawa, Indonesia. *Chemical Geology, 466*, 159-172. https://doi.org/10.1016/j.chemgeo.2017.06.004

Wen D. R., Chung S. L., Song B., Iizuka Y., Yang H. J., Ji J., Liu D., & Gallet S. (2008), Late Cretaceous Gangdese intrusions of adakitic geochemical characteristics, SE Tibet: Petrogenesis and tectonic implications. *Lithos, 105*, 1–11. https://doi.org/10.1016/j.lithos.2008.02.005

Weyer, S., & Ionov, D. A. (2007), Partial melting and melt percolation in the mantle: the message from Fe isotopes. *Earth and Planetary Science Letters, 259*, 119-133. https://doi.org/10.1016/j.epsl.2007.04.033

White, W. M. (2015), Probing the Earth's deep interior through geochemistry. *Geochemical Perspectives, 4*. https://doi.org/10.7185/geochempersp.4.2

Williams, H. M., Prytulak, J., Woodhead, J. D., Kelley, K. A., Brounce, M., & Plank, T. (2018), Interplay of crystal fractionation, sulfide saturation and oxygen fugacity on the iron isotope composition of arc lavas: An example from the Marianas. *Geochimica et Cosmochimica Acta, 226*, 224-243. https://doi.org/10.1016/j.gca.2018.02.008

Workman, R. K., & Hart, S. R. (2005), Major and trace element composition of the depleted MORB mantle (DMM). *Earth and Planetary Science Letters, 231*, 53-72. https://doi.org/10.1016/j.epsl.2004.12.005

Xu J. F., & Castillo P. R. (2004), Geochemical and Nd-Pb isotopic characteristics of the Tethyan asthenosphere: Implications for the origin of the Indian Ocean mantle domain. *Tectonophysics, 393*, 9-27. https://doi.org/10.1016/j.tecto.2004.07.028

Xu W. C., Zhang H. F., Luo B. J., Guo L., & Yang H. (2015), Adakite-like geochemical signature produced by amphibole-dominated fractionation of arc magmas: An example from the Late Cretaceous magmatism in Gangdese belt, south Tibet. *Lithos, 232*, 197–210. https://doi.org/10.1016/j.lithos.2015.07.001

Yin, A., & Harrison, T. M. (2000), Geologic evolution of the Himalayan-Tibetan orogen. *Annual review of Earth and planetary sciences, 28*, 211-280. https://doi.org/10.1146/annurev.earth.28.1.211

Yin, C., Ou, J., Long, X., Huang, F., Zhang, J., Li, S., et al. (2020), Late Cretaceous Neo-Tethyan slab roll-back: Evidence from zircon U-Pb-O and whole-rock geochemical and Sr-Nd-Fe isotopic data of adakitic plutons in the Himalaya-Tibetan Plateau. *Geological Society of America Bulletin, 132*(1-2), 409-426. https://doi.org/10.1130/B35242.1

Zhang L. L., Liu C. Z., Wu F. Y., Zhang C., Ji W. Q., & Wang J. G. (2016), Sr–Nd–Hf isotopes of the intrusive rocks in the Cretaceous Xigaze ophiolite, southern Tibet: Constraints on its formation setting. *Lithos, 258*, 133-148. https://doi.org/10.1016/j.lithos.2016.04.026

Zhang, X., Chung, S. L., Lai, Y. M., Ghani, A. A., Murtadha, S., Lee, H. Y., & Hsu, C. C. (2019), A 6000-km-long Neo-Tethyan arc system with coherent magmatic flare-ups and lulls in South Asia. *Geology, 47*, 573-576. https://doi.org/10.1130/G46172.1

Zhang Z. M., Dong X., Xiang H., He Z. Y., & Liou J. G. (2014), Metagabbros of the Gangdese arc root, south Tibet: Implications for the growth of continental crust. *Geochimica et Cosmochimica Acta, 143*, 268–284. https://doi.org/10.1016/j.gca.2014.01.045

Zhang Z. M., Zhao G. C., Santosh M., Wang J. L., Dong X., & Shen K. (2010), Late Cretaceous charnockite with adakitic affinities from the Gangdese batholith, southeastern Tibet: Evidence for Neo-Tethyan mid-ocean ridge subduction? *Gondwana Research, 17*, 615–631. https://doi.org/10.1016/j.gr.2009.10.007

Zhang Z., Ding H., Palin R.M., Dong X., Tian Z., & Chen Y. (2020), The lower crust of the Gangdese magmatic arc, southern Tibet, implication for the growth of continental crust. *Gondwana Research, 77*, 136-146. https://doi.org/10.1016/j.gr.2019.07.010

Zhang, S-Q., J. J. Mahoney, X-X. Mo, A. M. Ghazi, L. Milani, A. J. Crawford, et al. (2005), Evidence for a widespread Tethyan upper mantle with Indian-Ocean-type isotopic characteristics. *Journal of Petrology, 46*, 829–858. https://doi.org/10.1093/petrology/egi002

Zhao, M. S., Chen, Y. X., Xiong, J. W., Zheng, Y. F., Zha, X. P., & Huang, F. (2023), Element mobility and Mg isotope fractionation during peridotite serpentinization. *Geochimica et Cosmochimica Acta, 340*, 21–37. https://doi.org/10.1016/j.gca.2022.11.004

Zheng Y. C., Hou Z. Q., Gong Y. L., Liang W., Sun Q. Z., Zhang S., et al. (2014), Petrogenesis of Cretaceous adakite-like intrusions of the Gangdese Plutonic Belt, southern Tibet: Implications for mid-ocean ridge subduction and crustal growth. *Lithos, 190–191*, 240–263. https://doi.org/10.1016/j.lithos.2013.12.013

Zheng Y. F. (2019), Subduction zone geochemistry. *Geoscience Frontiers, 10*, 1223-1254. https://doi.org/10.1016/j.gsf.2019.02.003

Zhu, D. C., Wang, Q., Chung, S. L., Cawood, P. A., & Zhao, Z. D. (2019), Gangdese magmatism in southern Tibet and India–Asia convergence since 120 Ma. *Geological Society, London, Special Publications, 483*, 583-604. https://doi.org/10.1144/SP483.14

Zhu, D. C., Zhao, Z. D., Niu, Y., Mo, X. X., Chung, S. L., Hou, Z. Q., et al. (2011), The Lhasa Terrane: record of a microcontinent and its histories of drift and growth. *Earth and Planetary Science Letters, 301*, 241-255. https://doi.org/10.1016/j.epsl.2010.11.005